University of Windsor

Scholarship at UWindsor

2009

Wind Tunnel Study on the Aerodynamic Performance of Deflectors with Different Shapes

Yaoyao Zhang
University of Windsor

Wind Tunnel Study on the Aerodynamic Performance of Deflectors with Different Shapes

By

Yaoyao Zhang

A Thesis

Submitted to the Faculty of Graduate Studies through the Department of Mechanical,

Automotive and Materials Engineering in Partial Fulfillment of the Requirements for the

Degree of Master of Applied Science at the University of Windsor

Windsor, Ontario, Canada

2009

Canada

AUTHOR'S DECLARATION OF ORIGINALITY

I am aware of the University of Windsor Senate Policy on Authorship and I certify that I have properly acknowledged the contribution of other researchers to my thesis, and have obtained written permission from each of the co-author(s) to include the above material(s) in my thesis.

I certify that, with the above qualification, this thesis, and the research to which it refers, is the product of my own work.

I declare that, to the best of my knowledge, my thesis does not infringe upon anyone's copyright nor violate any proprietary rights and that any ideas, techniques, quotations, or any other material from the work of other people included in my thesis, published or otherwise, are fully acknowledged in accordance with the standard referencing practices. Furthermore, to the extent that I have included copyrighted material that surpasses the bounds of fair dealing within the meaning of the Canada Copyright Act, I certify that I have obtained a written permission from the copyright owner(s) to include such material(s) in my thesis.

I declare that this is a true copy of my thesis, including any final revisions, as approved by my thesis committee and the Graduate Studies office, and that this thesis has not been submitted for a higher degree to any other University of Institution.

ABSTRACT

The continuously increasing gasoline and diesel fuel costs generated immense interest in road vehicle efficiency. Because the aerodynamic drag of road vehicles is a major contributor to the fuel consumption at highway speeds, renewed interests ar e focusing on attempts to find novel drag-reducing technology

In this project, a newly designed air deflector with the shape of three concave surfaces was proposed. The effect of the deflector shape on the aerodynamic performance of a truck model, such as drag coefficient, was investigated. The results were compared to the same truck model with conventional convex deflector and without deflector. The relationship between the deflector shape and the drag force coefficient, as well as Reynolds number was revealed in all cases. The impact of deflector details on the characteristics of the airflow around the truck model, focusing on the wake area behind the trailer was also investigated.

ACKNOWLEDGEMENTS

TABLE OF CONTENTS

LIST OF TABLES

LIST OF FIGURES

NOMENCLATURE

A   Frontal area of the vehicle

A_N Cross-sectional area of wind tunnel testing section

A/D   Analogue/Digital

D   Diameter of the circular cylinder [m]

C_D Drag coefficient, $2F_D / \rho V^2 A$

C_p Pressure coefficient

CTA   Constant Temperature Anemometer

F_1 Drag force in a top string [N]

F_3 Drag force in a bottom string [N]

F_D Drag force, $C_D (\rho V^2 A/2)$ [N]

$F_{D\text{-}TOP}$ Streamwise tensile component in a top string [N]

$F_{D\text{-}BOTTOM}$ Streamwise tensile component in a bottom string [N]

$F_f = \mu F_n$ Friction between the tires of truck model and the elevated

F_n Normal force exerted between the surfaces

F_{Total} $2F_{D\text{-}TOP} + 2F_{D\text{-}BOTTOM}$ [N]

H   Height of the truck model [m]

I/O   Input/Output

L   Length of the truck model [m]

L_{plate} Length of the elevated plate [m]

$L_{cylinder}$ Length of the circular cylinder [m]

N   Sampling number

Re   Reynolds number, VL/ν

T	Thickness of the elevated plate [m]
Tu	Turbulence intensity $u_{rms}/\overline{U}$ (%)
U_m	Local mean velocity [m/s]
U_∞	Free stream velocity [m/s]
$\overline{U}$	Time averaged velocity [m/s]
u_{rms}	Root mean square velocity [m/s]
V	Mean flow velocity [m/s]
W	Width of the truck model [m]
W_{plate}	Width of the elevated plate [m]
X	Distance between model base and downstream Point for Velocity measurement [m]
3-D	Three-dimensional

Greek Symbols

$\alpha, \alpha', \beta, \beta'$	Geometrical angle of cylinder setup
ν	Kinetic viscosity [m^2/s]
ρ	Density [kg/m^3]
φ	Blockage ratio
μ	Coefficient of static friction

Chapter 1 INTRODUCTION

1.1 Project Background

On North American roads, truck population continues to grow in recent years. The large amount of potential fuel saving coupled with increasing fuel cost has spurred renewed interest in heavy-vehicle aerodynamics. From previous studies, it is known that aerodynamic drag is a significant parasitic loss in a typical tractor-trailer system operating at highway speed [Wood and Bauer, 2003]. For a typical heavy vehicle at a highway speed of 100km/h, the energy required to overcome aerodynamic drag is about 65% of the total expenditure [Mason and Beebe, 1978]. Furthermore, data released by the American Trucking Association indicated that the tractor/trailer interface contributes to approximately 20% of the total drag. Therefore, practical devices to reduce aerodynamic drag will offer a cost-effective opportunity to improve fuel economy.

Considerable efforts were made in the last few decades to study vehicle aerodynamics on full-scale, on road study and reduced-scale wind tunnel testing [Vexler and Katz, 1985], as well as computational fluid dynamics (CFD) simulation [Patel and Vijayakumar, 2001]. The results show that aerodynamic performance can be improved by alerting the bodylines on a vehicle. Its drag coefficient can be maintained at a minimum value by properly designing various component profiles [Hucho, 1998; Copper, 2003]. Based on those previous studies, tractor manufactures have made significant progress in reducing aerodynamic drag over the past three decades. Especially in recent years, research was focused on three areas within the tractor-trailer system: the tractor-trailer gap, trailer sides and trailer wake [Losito and Nicola, 1983]. A number of practical add-on devices to reduce aerodynamic drag for tractor trailers were designed and applied in real life.

1.2 Motivation

Though trucks represent a significant fraction of the vehicles on the road, it is surprising to note that the aerodynamic shape of the tractor-trailer, especially the tractor-mounted deflector, which is a critical drag-reduction facility, has remained largely unchanged compared to the passenger automobile over the past few decades. Significant opportunities remain to improve tractor-trailer aerodynamic integration and to offer robust, practical aerodynamic solutions to customers.

Due to the utilitarian function of trucks, it is unlikely that it will experience significant changes in the near future. However, this does not mean that trucks can not be improved in some manner that would be beneficial. The conventional air deflectors were based primarily on streamlining the shape of the add-on devices on top of tractors, while the aerospace industry has gone through stages of development with ingenious features such as winglets and grooves. Thus, it appears that new ideas may also be applied to air deflector design. The information of how the details of vehicle shape would affect its aerodynamic performance, especially under different flow conditions, should be investigated and supplied.

1.3 Objectives

In this project, a newly designed air deflector with the shape of three concave surfaces was proposed. A series of wind tunnel tests were conducted on a 1:24 scale truck model. Three cases were carried out to evaluate the impact of air deflector shape on the aerodynamic performance of a tractor-trailer.

1) Truck model with the proposed deflector
2) Truck model with the original deflector
3) Truck model without deflector

The objectives of the current study are as follow:

a) Compare the drag coefficient by using different air deflectors under smooth flow condition (Tu<0.55%).

b) Study the Reynolds number effect and yaw angle effect.

c) Investigate the characteristics of the wake bubble by changing different air deflectors; uncover the relation between the wake bubble and the drag force.

Chapter 2 LITERATURE REVIEW

2.1 Aerodynamic Drag Reduction of Heavy Vehicles

An assessment of the energy usage of tractor-trailer trucks (Figure 2.1) shows that the primary resistance forces are rolling friction and aerodynamic drag [Wood and Bauer, 2003]. Rolling friction is the resistance that occurs when a round object such as a tire rolls on a flat surface. It is caused by the deformation of the object, the deformation of the surface, or both. Additional contributing sources include surface adhesion and relative micro-sliding between the surfaces of contact. It depends very much on the material of the wheel or tire and the sort of ground. Additional factors include wheel radius, and forward speed. As shown in Figure 2.1, when the vehicle speed goes up, the force required to overcome both aerodynamic drag and rolling friction increases. However, the rate of increase in aerodynamic drag with increasing vehicle speed is much greater than that for rolling friction.
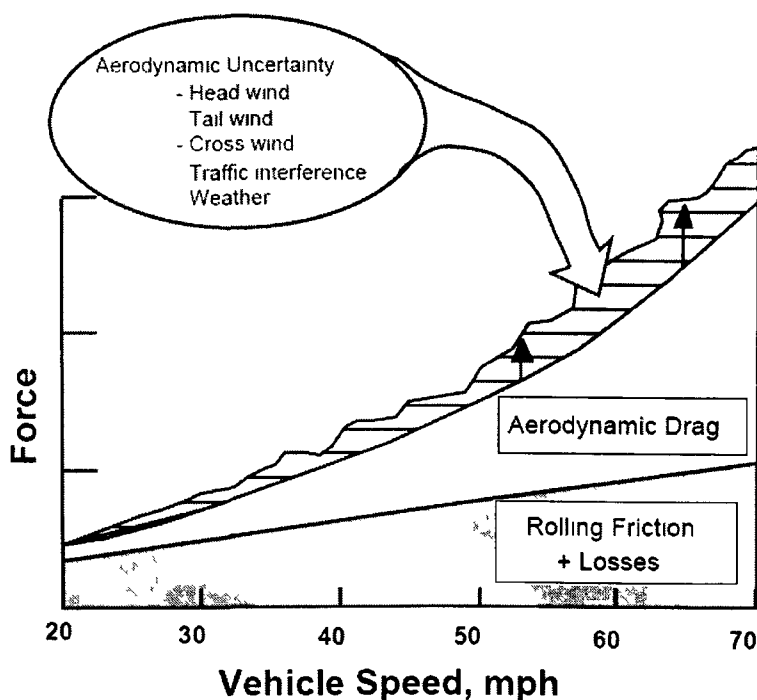
Figure 2.1 Graphic depicting the impact of aerodynamic uncertainty on horsepower
requirements for a heavy vehicle tractor-trailer truck [Wood and Bauer, 2003]

4

Figure 2.2 can be viewed as a summary of the aerodynamic drag reduction efforts for tractor-trailer vehicles over the past 20 to 30 years from Wood and Bauer's study [2003]. These data show the relative magnitude of the aerodynamic drag force on a tractor-trailer truck under ideal wind conditions. It can be seen that, the total aerodynamic drag consists of four main parts, the area in front of the tractor, the gap area, the tire area and the wake area.
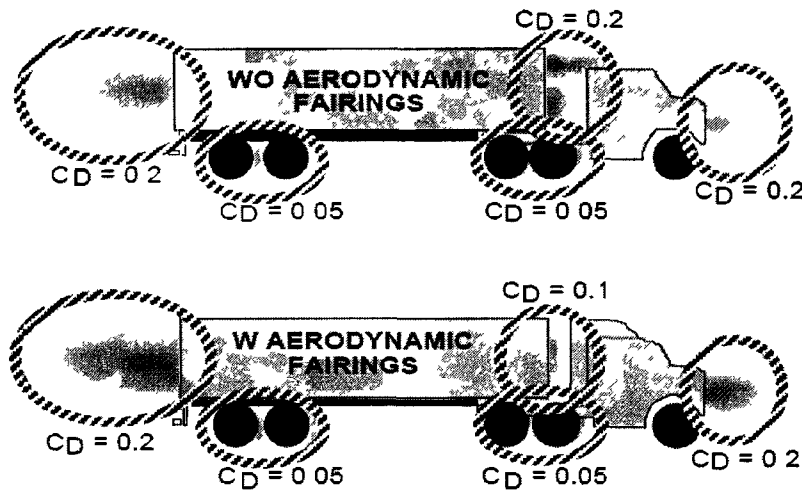
Figure 2.2 Distribution of aerodynamic drag for a heavy vehicle tractor-trailer truck, with and without aerodynamic fairings, operating in a zero crosswind condition. [Wood and Bauer, 2003]

In the gap area, after utilizing aerodynamic fairings on the tractor to direct the flow away from the trailer front face, the aerodynamic drag on the tractor has been reduced. These efforts have produced reductions in the aerodynamic drag of 30%, for an operating speed of 96 km/h, with corresponding improvements in fuel economy approaching 15% [Wood and Bauer, 2003].

In the past few decades, Cooper [2003] has made a significant contribution in this area, to re-explore the technology developed to reduce drag force on truck, demonstrate and compare their benefit. Based on this work, two generation of drag reduction devices were summarized.

First Generation drag reduction devices

In the late 1970's and early 1980's, considerable effort was expended in the first generation drag reduction device, which are the add-on aerodynamic aids to the cab or the trailer from improved cab shaping and from body/trailer front-end edge rounding.

a) Add-on Flat Plate

An example of a class of such devices was proposed by Saunder in 1966, as shown in Figure 2.3. The function of the plate is to shield the exposed face of the trailer by deflecting the air flow over the top and sides of the face, so that the separated shear layer from the edges of the plate matches to the perimeter of the trailer. Thus, the ideal size of plate is the smallest which will deflect the oncoming flow over the front face of the trailer. The experimental data showed that, when the separated shear layer from the edges of the plate matches to the perimeter of the trailer, the addition of the plate would reduce drag by 11%. When the small flow path between the roof-air unit and the roof was filled in with clay, the incremental drag reduction increased to 0.28, which is almost up to 30% off [Mason and Beebe, 1978]. The higher drag flow field with the roof-air unit shows that, the separated shear layer was intercepted by the trailer face. These results indicate that, when the shear surface from the tractor was matched to the trailer, it presented the optimum drag reduction.
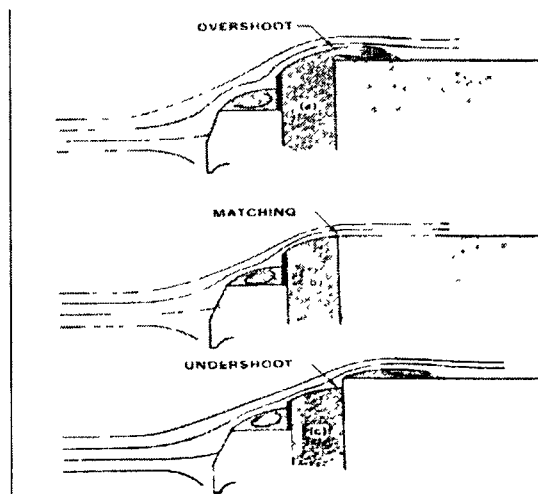
Figure 2.3 Sizing of roof-mounted plate for minimizing drag of tractor-trailer combination [Mason and Beebe, 1978]

b) Add on roof fairings

Figure 2.4 shows an example of another class of roof-mounted devices, which is introduced in Mason and Beebe's study [1978]. It is a very successful drag reduction device which is similar as the air deflector utilized by the on road tractor-trailer. The fairing eliminates the separation from the tractor roof that occurs with flat plate device, and avoids the local concave streamline curvature associated with that separation. At a norminal Reynolds number of 2×10^6 which was equivalent to 30km/h full-scale road speed, a low drag coefficient level of about 0.6 was reached for all configurations, regardless of the gap or tractor size and shape. Visualization of the flow fields showed good matching of the separated shear surface from the fairing to the trailer. Experiments in Mason and Beebe's study were conducted on a 1/7-scale tractor-trailer model.
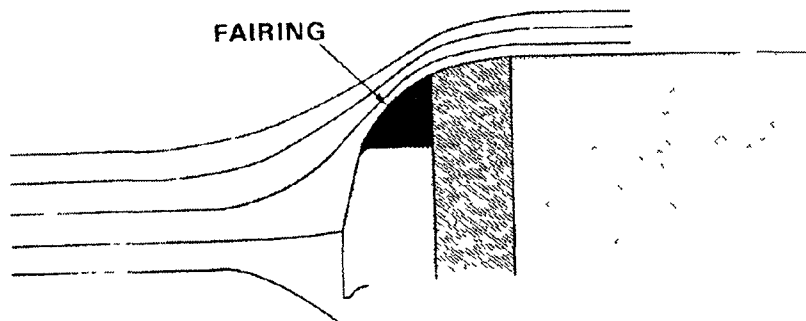
Figure 2.4   Optimum fairing for minimum drag when separated shear surface matched to trailer leading edges [Mason and Beebe, 1978]

Second Generation drag reduction devices

In the past twenty years, a mass of research work has been done to reduce the aerodynamic drag by adding the aerodynamic accessory devices, both by the full scale on-road study and small-scale wind tunnel study. For example, a series of programs achieved by Schoon and Pan [2006] and Schoon [2007] demonstrated significant fuel economy improvements for the devices developed for the tractor-trailer gap, trailer side skirting and trailer tapered aft section. An example of the second generation drag-reduction device is shown in Figure 2.5, which can improve the fuel economy up to 4.9% from on-road test using a real truck.
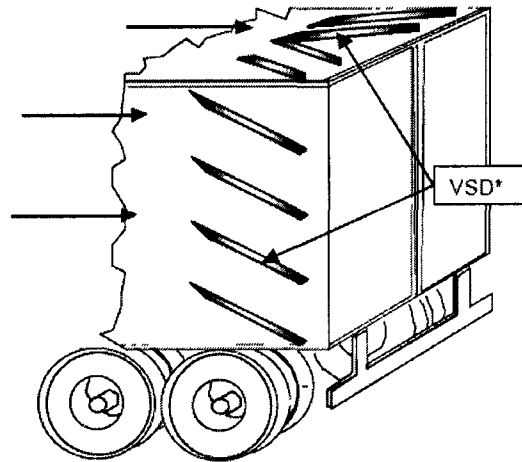
Figure 2.5 Sketch of the vortex strake trailer base treatment device installed on the aft portion of the trailer [Wood and Bauer, 2003]

But several of those second-generation drag reduction technologies investigated were not widely accepted because their individual economic return was smaller than those for cab deflector or body fairings. To sum up, it shows from previous work [Wood and Bauer, 2003] that the most significant drag reduction is achieved by the add-on air deflector.

*Full-scale studies

Generally speaking, for the full-scale studies of tractor-trailer on the aerodynamic performance, it can be divided into two types, one is on-road testing; the other is full-scale wind tunnel study.

a) On-road testing

The road-testing technique for the aerodynamic lift and drag measurements was found to be very practical, configuration changes were fast and simple to perform, and the results of test can be easily related to practical use, such as fuel saving. But the operational and environmental factors can during the on-road test have a dominating effect on the

aerodynamic drag of tractor-trailer trucks, such as interference from other vehicles, atmospheric effects, and road conditions.

A mass of research work has been done in this area during the past few decades. Wayne [2007]'s work provide information about emissions from in-use HDDVs (heavy-duty diesel vehicle) under typical driving conditions and can be used to better understand emissions inventories and in the development of regulations for in-use vehicles. A coast-down method has been developed by Bischof et al [2004], which is suitable for low-cost and easy-to-handle industrial application in the investigation of aerodynamic drag differences due to configuration changes. The analysis method-integration of the equation of motion- seems to be insensitive to environmental influences. The test vehicle chosen for this study was a BMW serial car; further investigation could be carried out by using commercial vehicle to reduce environment influence of the on-road testing.

To provide more applicable on-road testing information of tractor-trailer, Wood and Bauer [2003] have done a research work on aerodynamic drag reduction by using three low cost, simple, geometric devices which are designed and validated through operational testing. The data collection period in their study extended from July 2001 to March 2003 .The testing was performed in duplicate trailers which were operated with and without the aerodynamic drag reduction technologies through 232 Total Trips and 253600 Total Miles. The results show that these technologies have shown a combined fuel savings of approximately 10% at an average speed of 47.5 mph. This improvement in fuel economy correlates to an equivalent drag reduction of approximately 30% with a corresponding drag coefficient of 0.45.

From Vexler and Katz's study [1985], the comparison of the small-scale wind tunnel tests (which are considered to be less accurate) with the direct road-test data showed good agreement. The comparison with the low-Reynolds-number wind tunnel data showed good qualitative results, but both drag and lift increments due to geometric changes were larger in the full-scale tests. Small-scale tests are therefore useful to provide qualitative information about the influence of geometrical changes; they could be useful in

developing general configurations or for calibrating analysis prediction methods. For information about fine details of production automobile, however, full-scale (wind tunnel) testing is still the best way to go.

b) Full-scale wind tunnel study

The effectiveness of a drag reduction device-an aerodynamic boattail on a tractor-trailer road vehicle was measured in the NASA Ames Research Center 80-by 120-Foot wind tunnel (24.38-by 36.58-m) by Lanser et al in 1991. The results of this full-scale test indicated that, the aerodynamic boattail is effective for reducing the wind-averaged drag of a tractor-trailer by about 9.8% over a yaw range of ± 15 degree. The experiment carried out by truck models of 50% scale can also provided information of drag force and the surface pressure measurements, which is compared well to results obtained in full-size wind tunnel study [Monkewitz and Muller, 2008].

2.2 Characteristics of Air Deflectors Mounted on Tractor-Trailers

Figure 2.6 shows the air flow around a standard tractor -trailer with and without deflector. It can be observed that after the installation of air deflector, the aerodynamic characteristics of the airflow are changed distinctly. The airflow around the top and bottom of the truck becomes smoother, and consequently the aerodynamic drag is reduced [Du et al, 2003].

Figure 2.6 Air flow around a standard tractor –trailer without and with deflector
[Du et al, 2003]

Figure 2.7 illustrates the experimental results of drag reduction done by Berta and Bonis [1980] using a one-half scale tractor-trailer model with different shape deflectors. In this figure, a drag coefficient C_D of 0.863 is measured at $0°$ yaw angle by using the original vehicle. Some add-on deflectors were tested and optimized; a few of them are sketched in Figure 2.7 With the best air deflector in Berta and Bonis's studies (the 5th one on the right), a C_D reduction of 34.1% was acheived by applying a convex shape air deflector on a rounded corner and smooth-walled trailer.

C_D	C_D Reduction %		C_L	C_L Reduction %
0 863			0 656	2 4
0 663	23 2		0 629	27 1
0 660	23 5		0 820	4 2
0 657	23 8		0 673	22
0 666	22 6		0 568	34 1
0 680	2 1		0 609	29 4
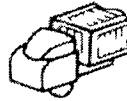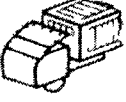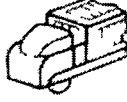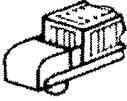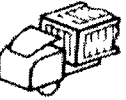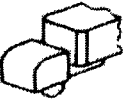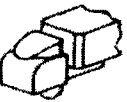
Figure 2.7 Tractor-trailer configuration: add-on devices and body-details study
[Berta and Bonis, 1980]

$\Delta c_D = 11\%$ $\Delta c_D = 28\%$ $\Delta c_D = 30\%$
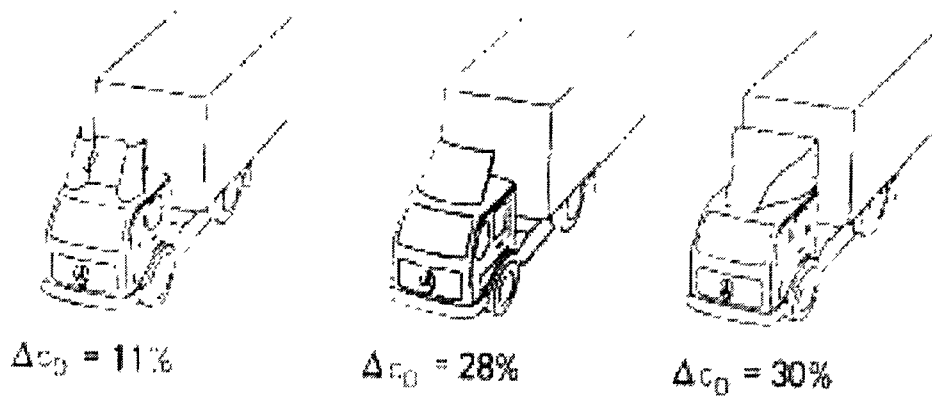
Figure 2.8 Drag reductions by applying the add-on devices with head-on airflow
[Hucho, 1998]

A whole range of add-on devices for reducing drag have been developed during the past few decades [Harris, 1980; Lanser et al, 1991; Engar, 2001; Storms et al, 2004; Surcel et al, 2008]. Some of those seen on the road are summarized by Hucho [1998] and illustrated in Figure 2.8. It is noticed that significant drag reduction was achieved by using different shape deflectors, but experimental details are still lacking, e.g., at which Reynolds Number a 30% C_D reduction can be obtained by using the 3rd deflector in Figure 2.8. To provide more information for application in real life, experimental details need to be investigated in a further study.

2.3 Application of Deflectors

On North American roads, the most common deflector shape is the convex surface deflector shown in Figure 2.9. Experimental results reported by NRC [2006] showed that, by using this kind of air deflector to change the stream direction and reduce drag force, a 28% C_D reduction and 13,000 liter fuel saving per year at 105 km/h can be achieved.

Figure 2.9 Convex surface air deflector

(http.//www.macsradiator.com/browseproducts/Kenworth-Charge-Air-Coolers.HTML)

A small portion of other shape deflectors can also be seen on the road, as shown in Figure 2.10. The deflector on the left is widely used in recent years.

Figure 2.10 Other shape deflectors on the road

(http://www.macsradiator.com/browseproducts/Kenworth--Charge-Air-Coolers.HTML)

2.4 Wind Tunnel Testing

A wind tunnel is a research tool developed to assist with studying the effects of air moving over or around solid objects. With the model mounted on a force balance, one can measure lift, drag, lateral forces, yaw, roll, and pitching moments over a range of angles of attack. This allows one to produce common curves such as lift coefficient versus angle of attack, and drag coefficient versus Reynolds number.

Since so far, the aerodynamic characteristics of a vehicle cannot be determined with reasonable accuracy by numerical methods, all computations predicting vehicle dynamics still are based on wind tunnel results [Hucho, 1998].

The advantage of wind tunnel tests is that data can be obtained on models (even in reduced scale) in a very early development phase, which allows an estimation of the dynamics of a vehicle concept long before drivable prototypes are available. However, wind tunnel tests can not perfectly simulate the on-road conditions. There are drawbacks listed below [Hucho, 1998].

a) On the road, a vehicle moves through a space of infinite dimensions ("free air"); in contrast, the dimensions of a wind tunnel test section are limited and comparatively small.

b) Instead of being quiet, a wind tunnel is extremely noisy if no specific precautions are taken during its design.

c) Generally, the relative motion between vehicle and road is not reproduced. The same is true for the rotation of the wheels.

2.4.1 Reynolds Number Effect

Generally speaking, the advantages of working with reduced-scale models are realized only if the results achieved with them can reliably be transferred to full scale. Dynamic similarity can lead to this target, that is, the Reynolds number of the reduced-scale test should match with the real life scenario [Baker and Brokie, 1991].

The scaling problem is frequently encountered in the aerodynamic research field since most wind tunnels are not big enough to accommodate full scale vehicles. The results from scaled models may be very misleading since the kinematic similarity can not be met [Vexler and Katz, 1985]. On the other hand, due to the high cost and uncontrollable environmental conditions, there are rare cases in which a full scale vehicle can be ground tested at operational speed. So methods of extrapolation are very important [Barlow et al, 1999].

There are generally two paths leading to this target: Reynold's law has to be strictly observed or by making use of other effects, a higher Re can be simulated. In 1989, Wiedemann [1989] proved that for a complex configuration like road vehicle, it is effective to manipulate the turbulence of the oncoming flow in order to decrease the "effective" Re. More specifically, when a screen of adequate mesh and bar size in the wind tunnel inlet is used, pressure distribution corresponding to different Reynolds numbers nearly fall onto a single curve that is equivalent to an increase of the effective Reynolds number, see Figures 2.11-2.13 for details.
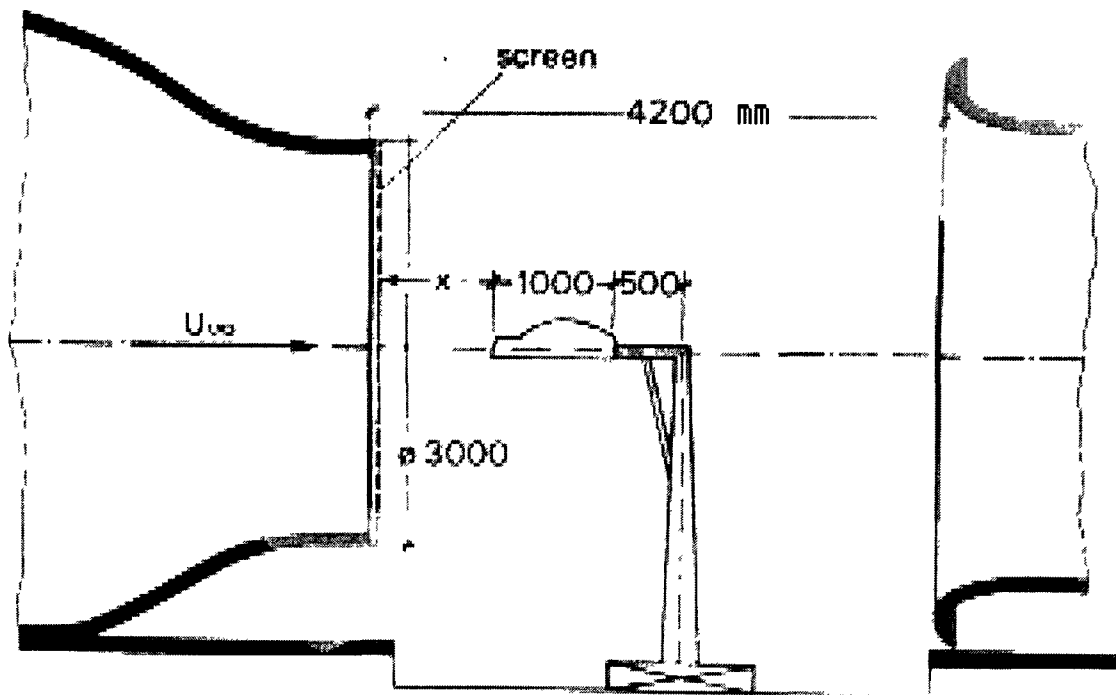
Figure 2.11 Setup of road vehicle in the open test section [Wiedemann, 1989]
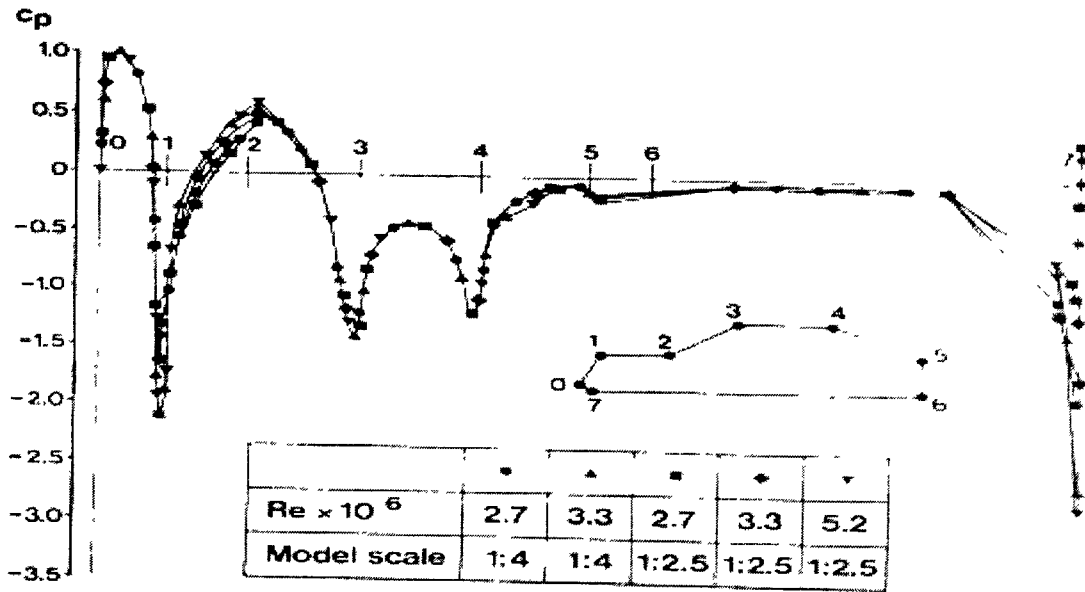
Figure 2.12 Pressure distribution on a road vehicle at different Re: no screen
[Wiedemann, 1989]

Re × 10^6	2.7	3.3	2.7	3.3	5.2
Model scale	1:4	1:4	1:2.5	1:2.5	1:2.5
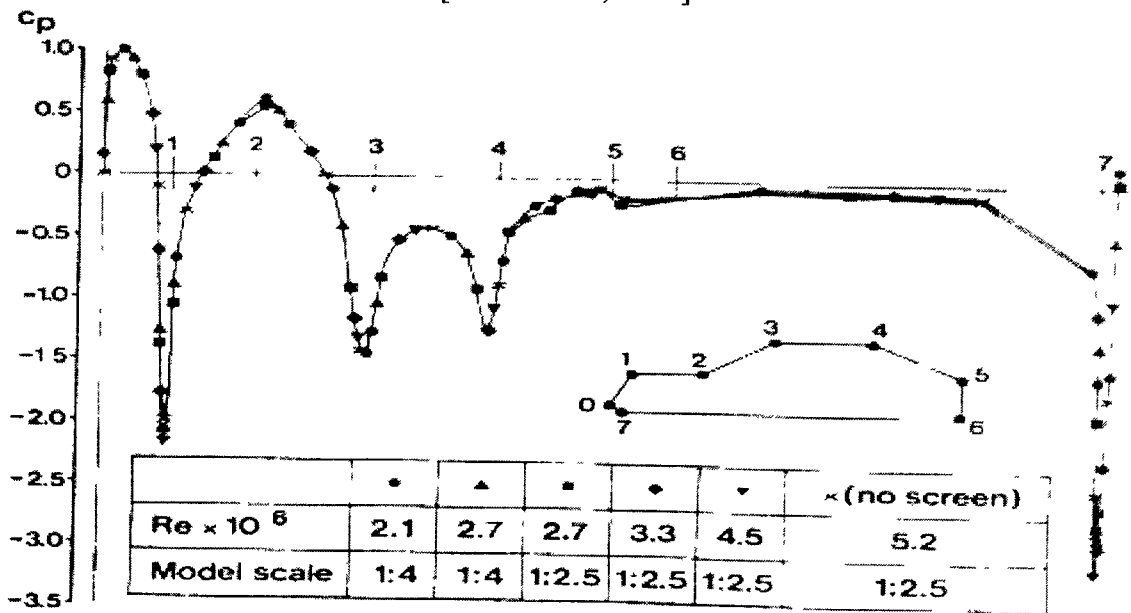
Figure 2.13 Pressure distributions on a road vehicle at different Re: Turbulence modified
by a screen [Wiedemann, 1989]

Re × 10^6	2.1	2.7	2.7	3.3	4.5	5.2 (no screen)
Model scale	1:4	1:4	1:2.5	1:2.5	1:2.5	1:2.5

There is a strong dependence of the pressure coefficient C_p on the Re, as can be seen in Figure 2.12. Figure 2.13 shows the pressure distribution for the same range of Re but with a screen mounted at the inlet. This time the results nearly fall onto a single line, which means there is no significant Re effect on pressure distribution if a screen is

applied. Moreover, it shows that the results of C_p at Re=5.2×10^6 without screen case and Re=2.7×10^6 with screen case are almost identical.
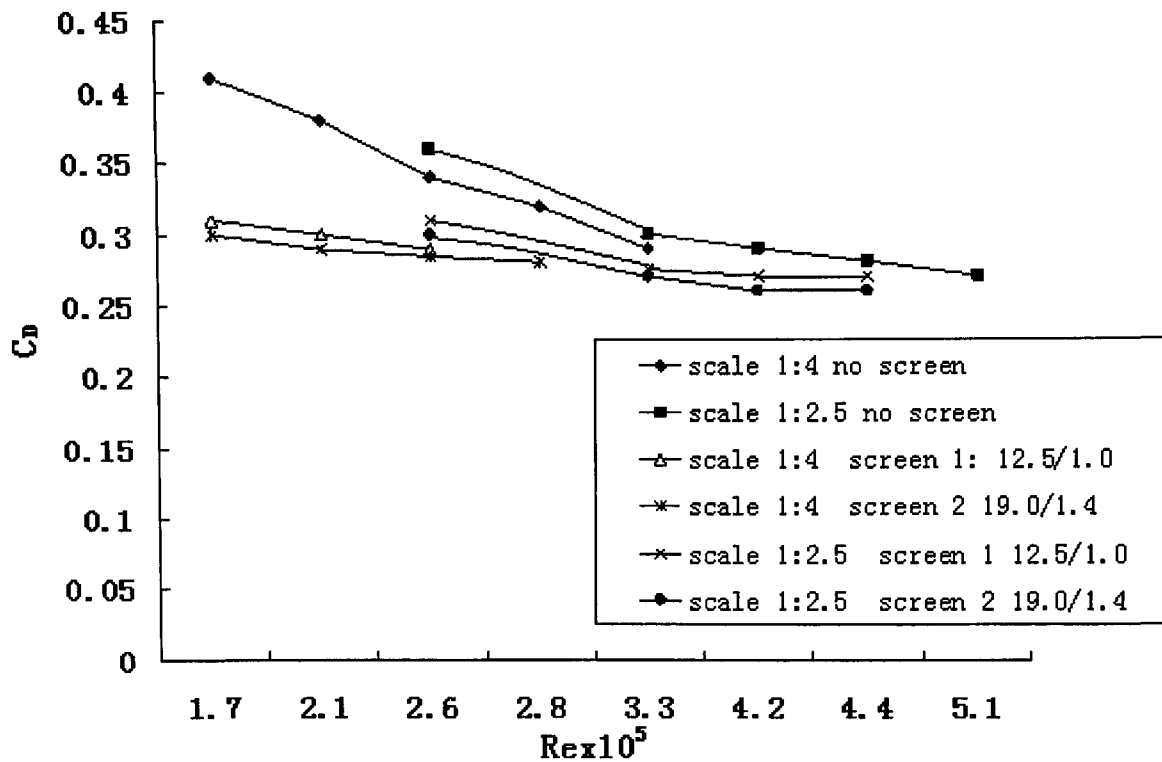
Figure 2.14 Drag coefficient of a road vehicle without ground plane vs. Re

For the drag coefficient measurement, see Table 2.1.

Table 2.1 Increasing the effective Re by screen application

Screen mounted at the wind inlet	Increase the effective Re by a factor of [Pressure distribution on the model vehicle]	Increase the effective Re by a factor of [Drag coefficient]
Screen 1	1.93*	1.52
Screen 2	1.93	1.73

* The result at Re=2.7×10^6 with screen is equivalent to the result of C_D at Re=5.2×10^6 without screen mounted at the wind tunnel inlet. Thus the effective Re can be increased by a factor of $5.2\times10^6/2.7\times10^6$=1.93.

2.4.2 Yaw Angle Effect

The drag coefficient at zero yawing angle is equal to driving in still air, which gives insufficient indication of aerodynamic characteristics in real operation, where the yaw angle effect must be taken into account. All vehicle types, with the exception of the light van, show a considerable increase in C_D with increasing yawing angle (Figure 2.15).
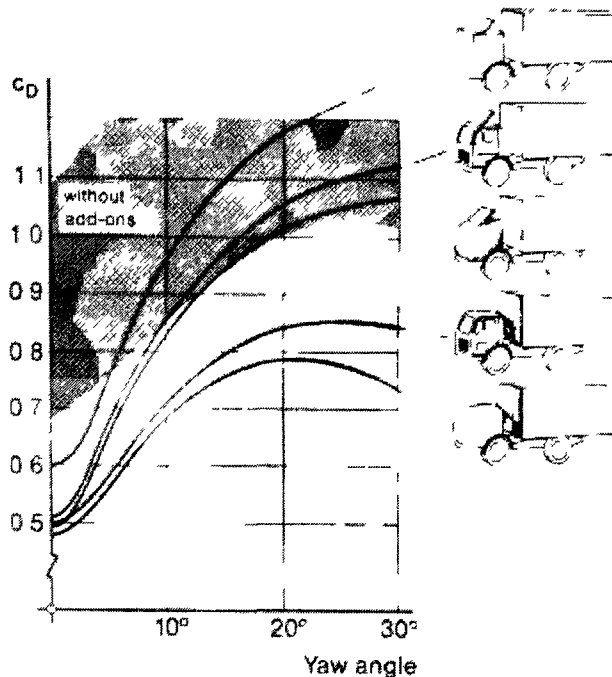
Figure 2.15 Drag reductions versus yaw angle through add-on devices

[Roy and Srinivasan, 2000]

2.4.3 Turbulence Effect

For most wind tunnel tests of vehicle aerodynamics, they are usually conducted in extremely low-turbulence wind tunnel (turbulence intensity Tu <1%), which is contradicted with reality. Because of this, the turbulence environment experienced by ground vehicles is currently not well understood. It causes increasing concerns about potential differences in aerodynamic behavior measured in steady flow wind tunnel conditions and that for vehicles on the road. As techniques and tools become available for better simulation of on-road conditions, there is a growing practical value in understanding what range of turbulence conditions are important to simulate

Previous research showed that turbulence was an important factor in the aerodynamic performance of cars in the real world.

Watkins [1990] studied the effect of turbulence on drag reducing devices for trucks, by comparing a series of on-road tests with those performed with scaled models in the wind tunnel under various levels of grid generated turbulence. He found that tunnel measurements obtained in smooth flow would consistently over-predict on-road drag coefficient reductions caused from add-on aerodynamic devices, especially at high yaw angles. But when the levels of wind tunnel turbulence were raised using grids, drag reductions from the aerodynamic devices were closer to those measured on-road. For those add-on deflectors, which are relied on a stable wake to shield the load, turbulence simulation should be investigated to correct the discrepancy between the tunnel and on-road results.

Carlino [2004] presented results that showed the addition of turbulence and a more representative velocity profile increases both the lift and the drag. Some of its effects on drag reducing devices, fluctuating side glass pressures, front lift forces and the aero-acoustic noise have been studied [Wordley and Saunders, 2008].

2.5 Wake Structure of a Tractor-Trailer

As illustrated before, the total drag force of a typical tractor-trailer consists of 4 parts. One of those is formed in the wake area, where two distinct wake features are present, a near wake and a far wake. The near wake is a recirculating region bounded by the shear layers emanating from the separated boundary layer from all sides of the body.

Figure 2.16 shows the near wake region of a typical Ahmed body: "A" and "B" are the two recirculating r egions; "C" is the longitudinal vortex, the "separation bubble" is indicated by "D" Both "A" and "C" depend mainly on the slant angle while "B" depends primarily on the ground clearance gap [Ahmed et al, 1984]. For a model without slant angle, which is the case considered in this study, the vortex "C" hardly occurs. Ahmed body is a simple model which can provide the strong three-dimensional flow in the front,

relative uniform flow in the middle and large structured wake at the rear of a real passenger car, without worrying about the unique features associated with different vehicle models.
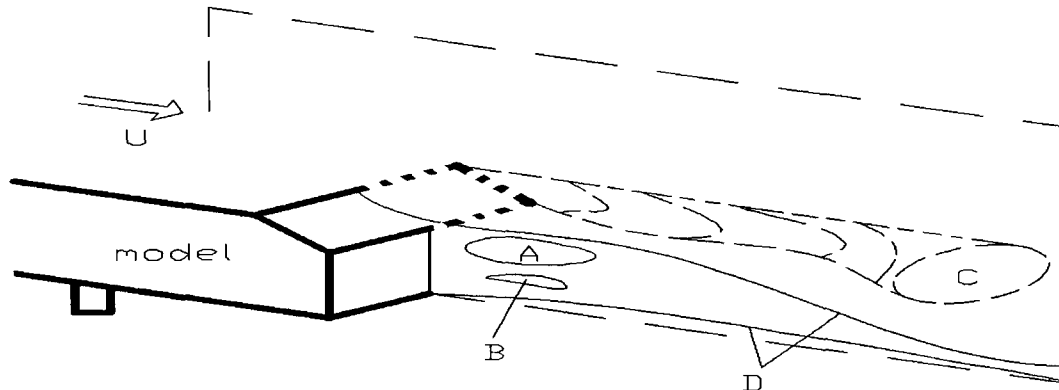
Figure 2.16 Horse shoe vortex system in the near wake region of an Ahmed body

[Yang, 2008]

For a simplified view of a typical wake structure from a blunt bluff body similar to that of the trailer end of a tractor-trailer vehicle. The furthest downstream point in the near wake is called the "free stagnation" point and it has a length of X_r measured from the model base to the free stagnation point, which is shown in Figure 2.17.
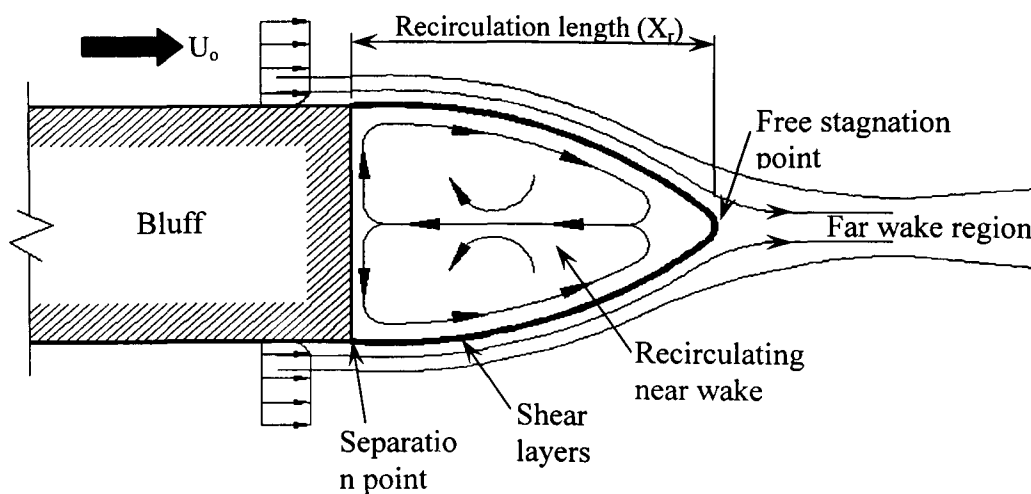
Figure 2.17 General wake structures behind a blunt axisymmetric body

[Adapted from Duell 1993]

One of the most important parameters to describe the wake characteristic is the recirculation length, which is defined as the distance between the model base and the mean location of the free stagnation point. The location of the time-averaged free stagnation point can be deduced from the minimum of U_m/U_∞, (where U_m is the local mean velocity and U_∞ is the free stream velocity) or, the maximum of the root mean square fluctuating velocity intensity.

The near wake velocity distribution determines the near wake size and locates the free stagnation point. By connecting all the stagnation points collected from the velocity distribution in near wake region, a "wake bubble" can be obtained. The shape of this "wake bubble" is based on the details of the truck model. In Yang's study [2008], four models with different shapes were utilized (Figure 2.18); the impact of truck model details on the characteristics of the wake bubble was investigated.

(a) Rectangular block (1:24)   (b) Rounded front model (1:24)

(c) Generic model (1:24)   (d) Scaled specific model-Kenworth (1:24)
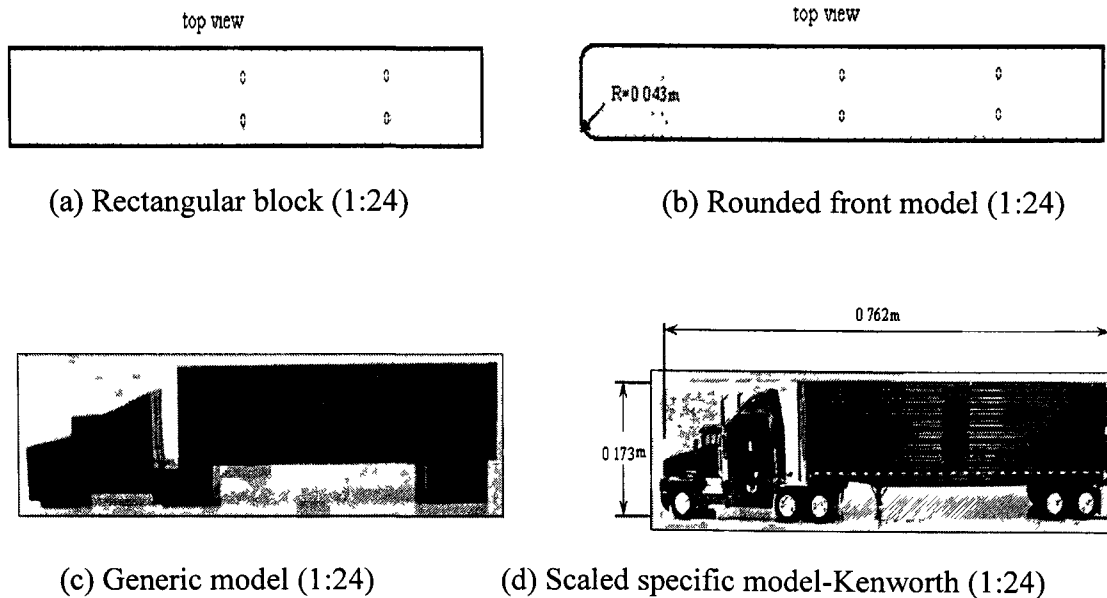
Figure 2.18 Four models with different shapes [Yang, 2008]
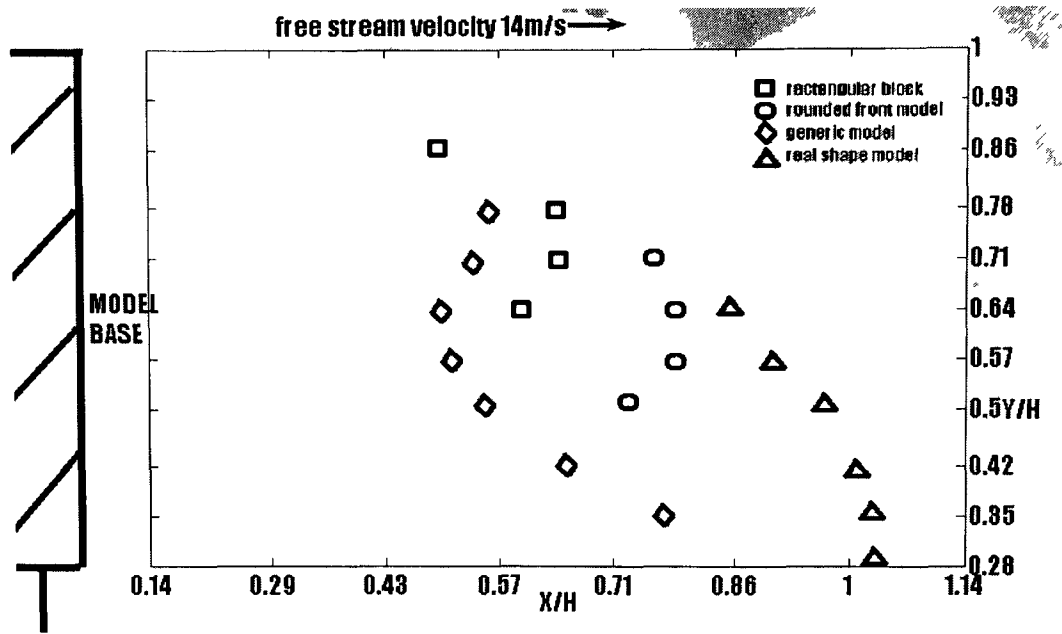
Figure 2.19 Comparison of bubble shapes of all the truck models
[Yang, 2008]

The experimental results in Yang's study, as shown in Figure 2.19, indicated that, the real shape model had the longest near wake region in the streamwise direction, while the rectangular block had the shortest. The length of the wake bubble of the rounded front model was literally identical to that of the generic model, and they were larger than the wake bubble of the rectangular block but shorter than that of the real shape model. Concerning the shape of the wake bubble, the bubble moved downward and away from the model base as more model details are included. The generic model appeared to show a double- (or dual-) bubble, but this has not been confirmed in the real truck model case. Based on Yang's study, it can be concluded that the details of the truck model shape had significant impact on the wake characteristics. As a subsequent research, it is believed that by changing the shape of the frontal area of the truck model, which is the deflector shape in this study, a considerable impact on the wake characteristic can also be observed and should be investigated in details.

Chapter 3 EXPERIMENTAL DETAILS

3.1 Wind Tunnel

The work presented here was carried out in a closed loop wind tunnel at the University of Windsor. The test section is 75 cm high and 75 cm wide at the inlet with a working length of over 4 m. To accommodate for boundary layer built up, the test section expands to 77 cm high and 76.5 cm wide at the end. The maximum attainable velocity in the empty test section was approximately 15 m/s. A preliminary test carried out at a mean velocity of 10 m/s showed a background turbulence intensity of less than 0.55% at the inlet of the test section in the absence of turbulence producing perforated plates. The wind tunnel used for conducting this experimental study is shown in Figure 3.1. The blockage ratio is of 3.2%, which is less than the 5% blockage ratio suggested by previous investigators [Gross and Sekscienski, 1966; Hucho, 1998].
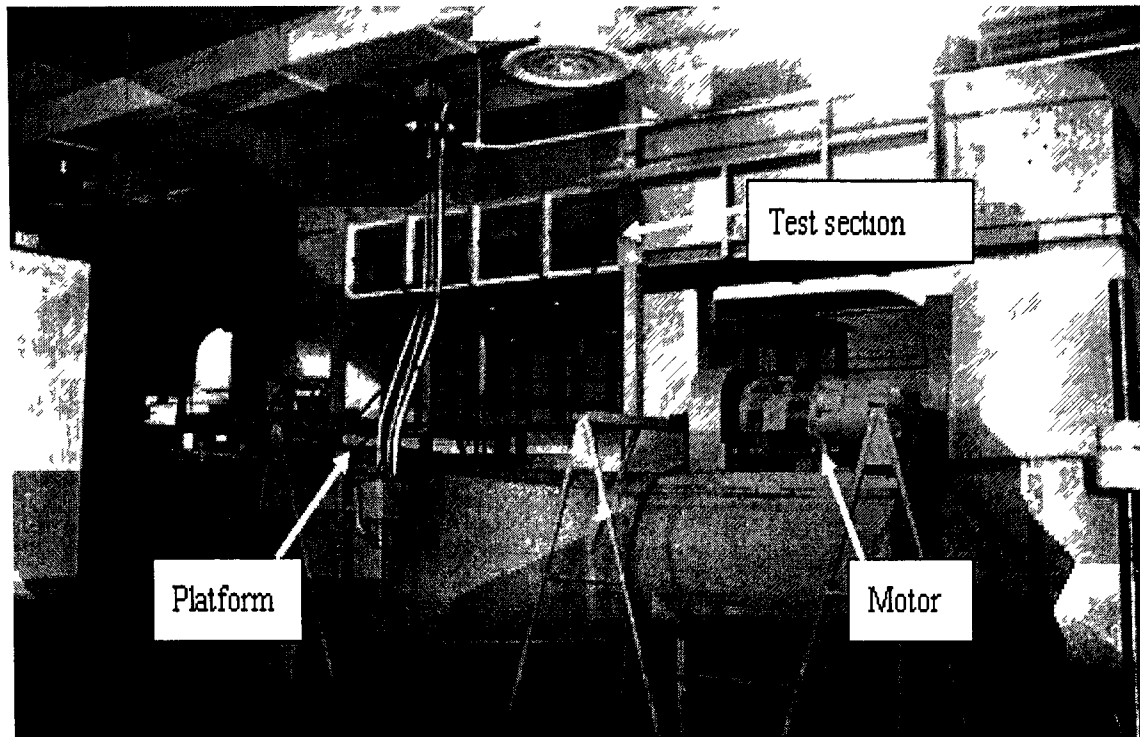
Figure 3.1 Closed-loop wind tunnel

3.2 Air Deflectors and Truck Model

<u>Air Deflectors</u>

The conventional deflector with a convex surface (Figure 3.2 (a)) is widely used by truck companies in recent years. To bring new ideas to deflector design, some different shape deflectors are proposed in this project to investigate their aerodynamic characteristic. The deflectors have flat surface but with different inclination angles were studied first. Figure 3.2 (b) shows a deflector with 30 degree inclined flat surface. Figure 3.2 (c) shows a deflector with 45 degree inclined flat surface. For further investigation, a new idea which is contrary to the convex deflector is proposed. Figure 3.2 (d) shows a deflector with three concave surfaces. Base on the previous study in this area [Hucho, 1998], a deflector with two concave surfaces on both of the side planes can reduce the drag coefficient up to 30%, which means a significant fuel saving. Considering the airflow around the surfaces of the truck model (Figure 2.6), the concave surface is supposed to change the aerodynamic characteristic of airflow distinctively and thus reduce the drag force on truck, especially in a yawing wind condition. To evaluate the effectiveness of the drag reduction by using concave surface deflector, and provide more experimental detail in this field, the new shape deflector of three concave surfaces is proposed. All deflectors have the same height which is designed to eliminate the flow separation in the gap region. Tuft flow visualization will be carried out for all those cases to evaluate the effect of the deflector shape on the airflow characteristics around the truck. The dimensions of different deflectors are shown in Figure 3.3.

(a) Convex surface deflector

(b) Deflector with 30 degree inclined flat surface
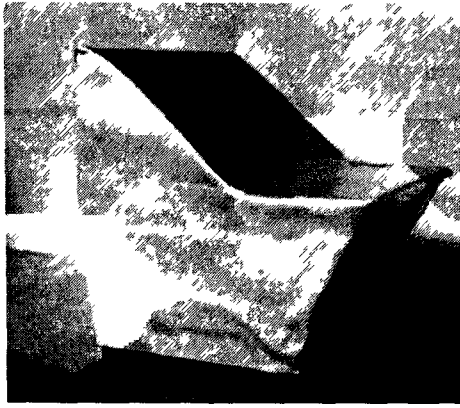
(c) Deflector with 45 degree
inclined flat surface
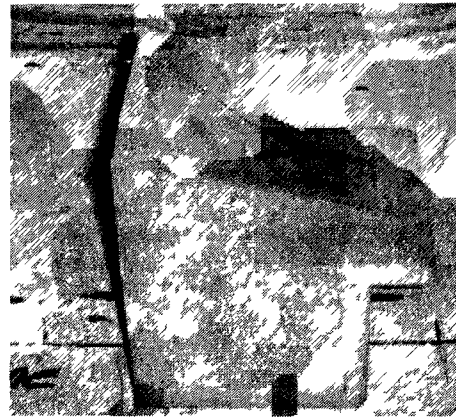
(d) Deflector with three concave surfaces

Figure 3.2 Four different shape deflectors
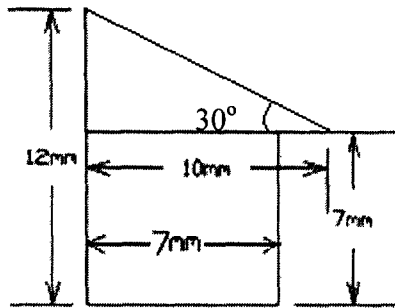
(a) 30 degree flat surface deflector
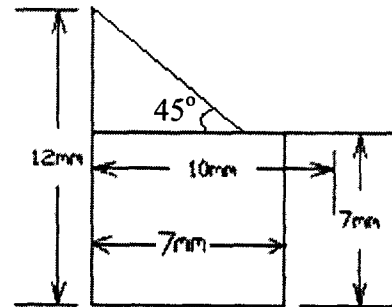
(b) 45 degree flat surface deflector
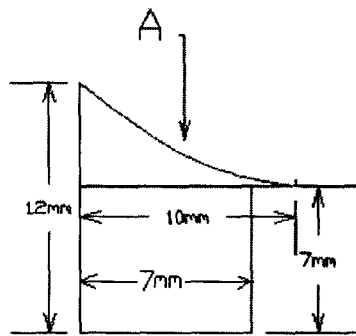
Side view
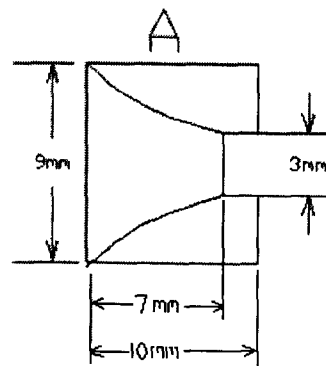
Plan view

(c) Proposed concave surface deflector

Figure 3 3 Dimensions of different deflectors

Truck Model

a) Original Kenworth T-600 Truck Model

Three cases of drag force measurement were performed in the wind tunnel tests, using an existing 1:24 scale truck model of a Kenworth T-600 Tractor with a Great Dane box trailer. The size of the model varies in length depending on the scale size, which is a simple reduction in size and is basically fractions of the actual size of a tractor-trailer. A tractor-trailer that is a 1:24 scale means that it is 1/24th the size of the actual truck in length, which is 60 feet (18.288m) long in "real life", and 2.5 feet (0.762m) long of the scaled truck model.

The overall dimension of the truck model is 0.173m (Height) ×0.108m (Width) ×0.762m (Length), as shown in Figure 3.4.
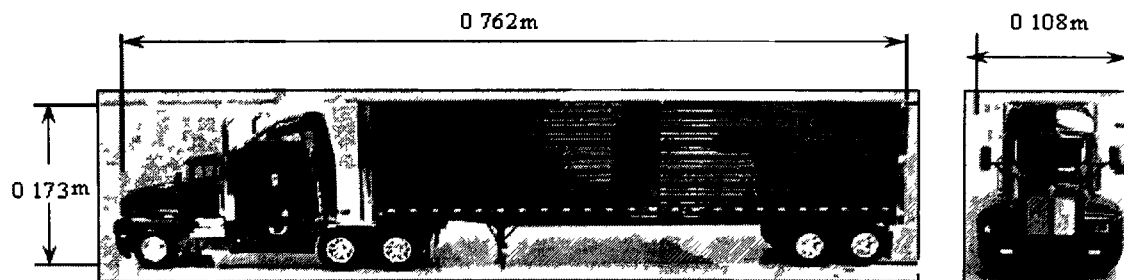
Figure 3.4 Side and front views of the 1:24 scale Kenworth truck model

After the experiments of tuft flow visualization, three cases were carried out by attaching different deflectors on the same truck model. In the first case, the original deflector with conventional convex surface was mounted on the top of the tractor, as shown in Figure 3.5. Figure 3.6 illustrates the proposed air deflector, of which all three faces have a concave surface. The third case of drag data was collected using the same truck model but without a deflector, as shown in Figure 3.7 The tractor-trailer gap for this study was held constant and equivalent to a full-scale of 101.6 cm.
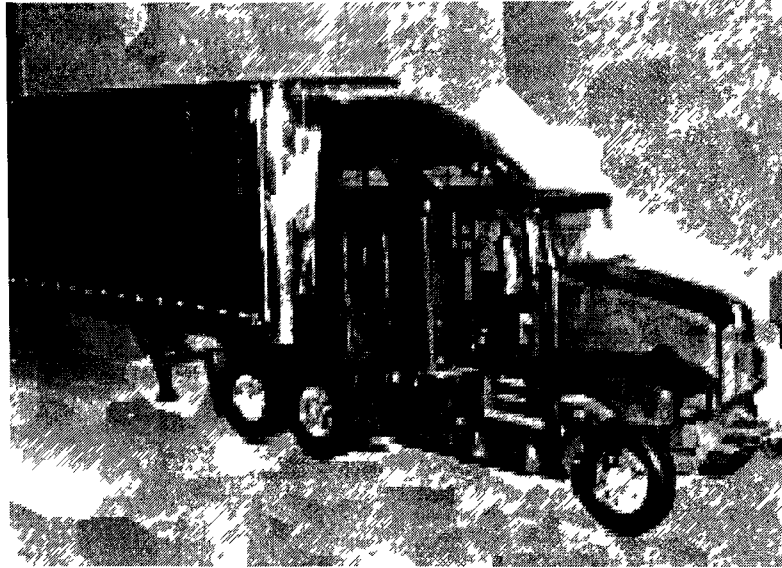
Figure 3.5 Conventional deflector with convex surface
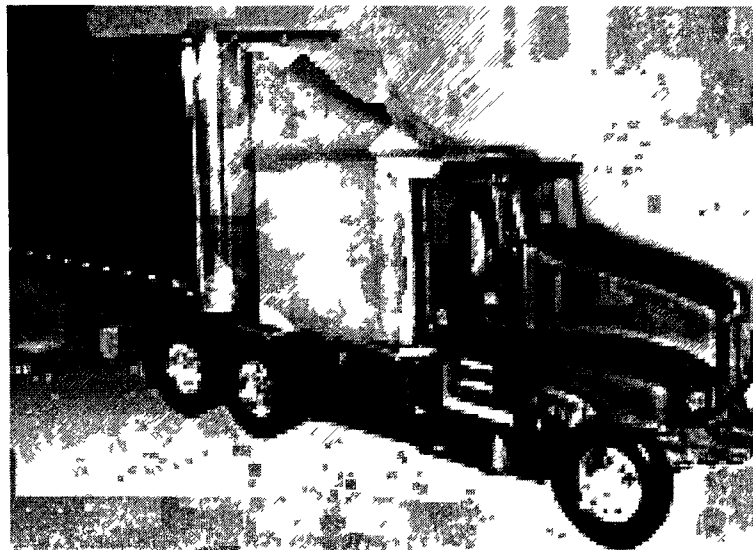
Figure 3 6 Proposed concave surface deflector
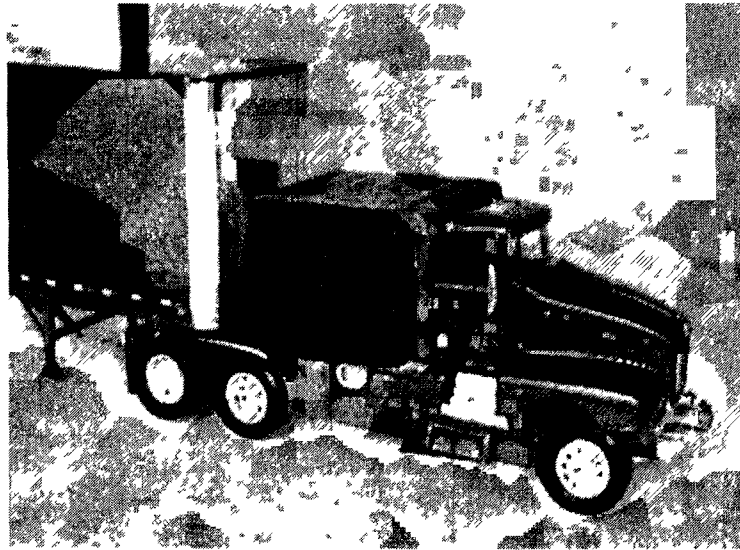
Figure 3.7 Truck model without deflector

3.3 Hot-wire and Load cell System

Hot-Wire System

The velocity measurements were carried out using a single normal hot-wire probe of DISA type 55P11. The hot-wire anemometer used in this experiment is a Dantec Streamline 55C90 CTA module installed within a Dantec 90N10 frame. The sensor on the probe is 1.25mm long, platinum-coated tungsten wire with a diameter of $5\mu m$. The signal was sent to the computer via a National Instrument ATMIO-16E-10 multifunction data acquisition board with a 12-bit resolution at a sampling rate of 40 kHz and low passed at 10 kHz to avoid the aliasing problem.
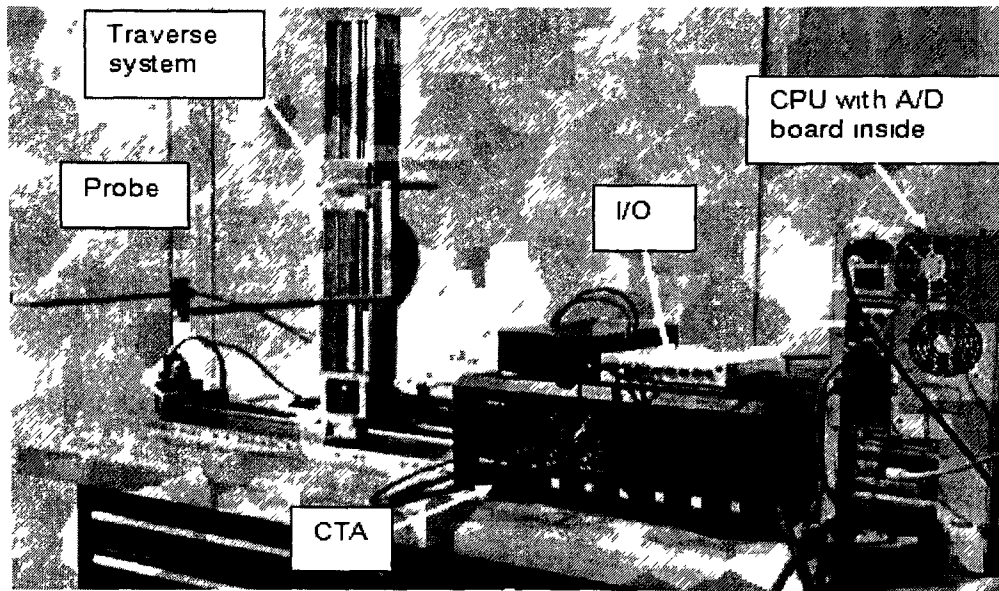
Figure 3.8 Hot-wire system [CTA: Dantec Streamline® 55C90, I/O· shielded I/O connector]

Load Cell System

The truck model was attached to a load cell secured onto the wind tunnel floor to quantify the drag force. The load cell used in this experiment is an ELG-V-1N-L03M ENTRAN model, which can measure tension or compression force. It has a full scale reading of 1 N, and an over-range limit of 10 N. It was connected to a model MROJHHSG Electro-Numeric Amplifier, which provided a 10 V excitation to the load cell.

3.4 Experimental Setup

Drag Force Measurement

To minimize the impact on the flow, the load cell was attached to the wind tunnel floor, located in front of the elevated plate, which was used to reduce the boundary layer effect (Appendix E). It was connected to the truck model by using a cord, with a certain angle to the wind tunnel floor, which was measured to calculate drag force. A pitot-static tube was secured at the inlet of the wind tunnel, to measure the free stream velocity during the test. A piece of wax paper was place between the tires of the truck model and elevated plate to reduce the friction The blockage ratio in this experimental setup is 3.3%, which

is less than the upper limit of 5% blockage ratio, beyond which corrections of blockage effect should be applied (Appendix F). The set up is shown schematically in Figure 3.9.
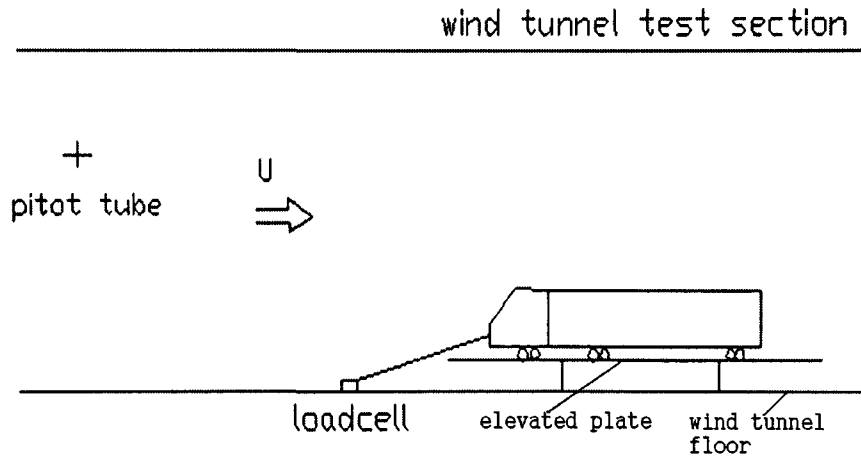
Figure 3.9 Experimental setup for drag force measurement

During the experiment of drag force measurement, the truck model was not rotating or sliding. Because the free stream velocity was relatively low in this experiment. The friction between the tires of truck model and the elevated was calculated from the following equation,

$$F_f = \mu F_n$$

Where μ is the coefficient of static friction, which is different from the coefficient of kinetic friction when the tires are rotating. F_n is the normal force exerted between the surfaces, which is the self-weight of the truck model in this study.

<u>Wake Measurements</u>

This series of wind tunnel tests aims at studying the impact of different shape air deflectors on the wake characteristics. The truck model was placed right along the central line of the wind tunnel section, on an elevated plate (Figure 3.10). The testing area covered the vertical central plane right behind the truck model. During the tests, a single hot-wire probe was mounted (along with a temperature probe for correcting the fluid

density and viscosity deviation from the calibrated conditions) on the traverse system downstream of the model, the movement of which was controlled by a smart motor program.
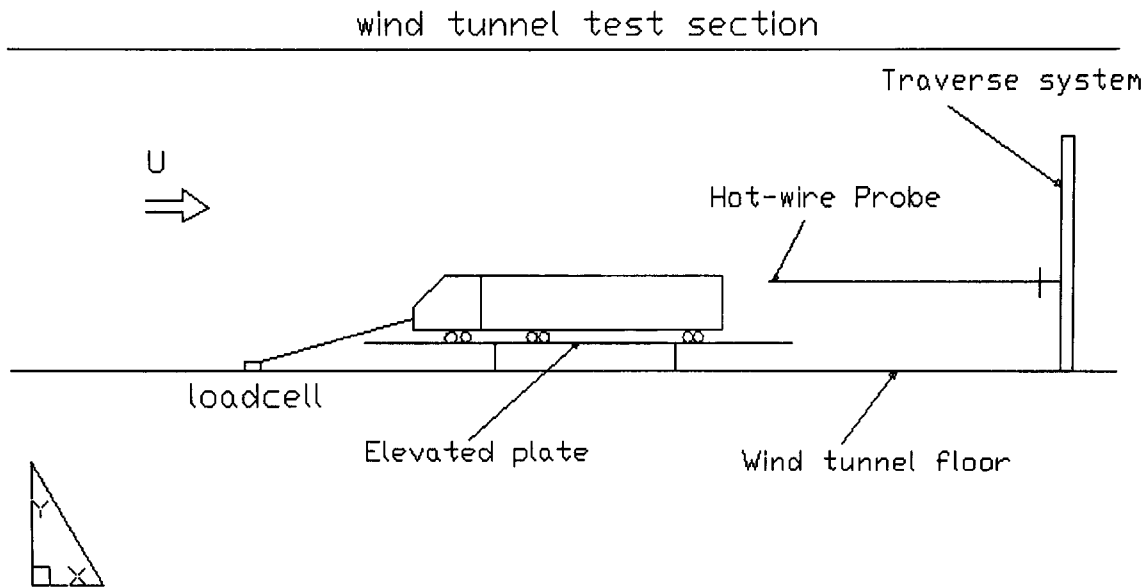
Figure 3.10 Experimental arrangements for studying wake of the truck model

First, the near wake velocity distribution were measured in the centre plane to investigate the characteristics of the wake bubble, then experiments were repeated by using the original deflector and the proposed deflector in side planes, to reveal 3D feature of the wake bubble. The location of the side planes were chosen at $Z=\pm 1$ inch (0.0254m), $Z=\pm 2$ inch (0.0508m), where Z is the distance from the side plane to the central plane.

The grid systems used for hot-wire measurement are illustrated in Figure 3.11. The starting position of the probes was 1 inch (0.0254m) downstream from the model base, in order to avoid potential probe breakage. The area covered was 5.5 inch (0.14m) in width and 5.5 inch (0.14m) in height. The height of the area covered by the testing grid was the same as that of the trailer.

Two sets of grid systems were used to collect points. Firstly, 121 points were measured in the first grid system (11x11); the interval between each two points was 0.5 inch (0.0128m). Then, moved the starting point 0.25 inch (0.0064m) further downstream, another 121 points were measured in the second grid system (11x11); the interval between each two points was 0.5 inch (0.0128m). Thus, 242 points were measured totally for each section to make sure enough points would be collected to get the precise velocity distribution in wake area. The interval between each two horizontal points was 0.25 inch (0.0064m); between each two vertical points was 0.5 inch (0.0128m).
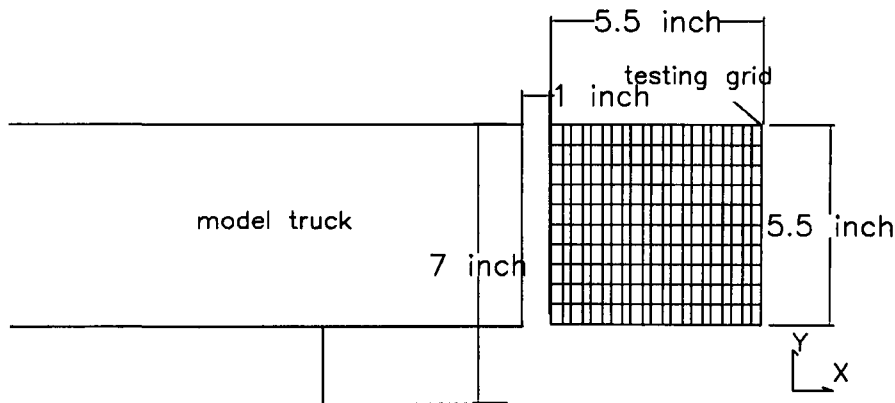
Figure 3.11 Grid for data collection

Chapter 4 RESULTS AND DISCUSSIONS

4.1 Tuft Flow Visualization

The airflow around the tractor-trailer is related to the magnitude of the drag force in that area [McLandress et al, 2001], a series of tuft flow visualization tests [Villanueva, 2002] were carried out to investigate the flow pattern around truck model when using different deflectors.
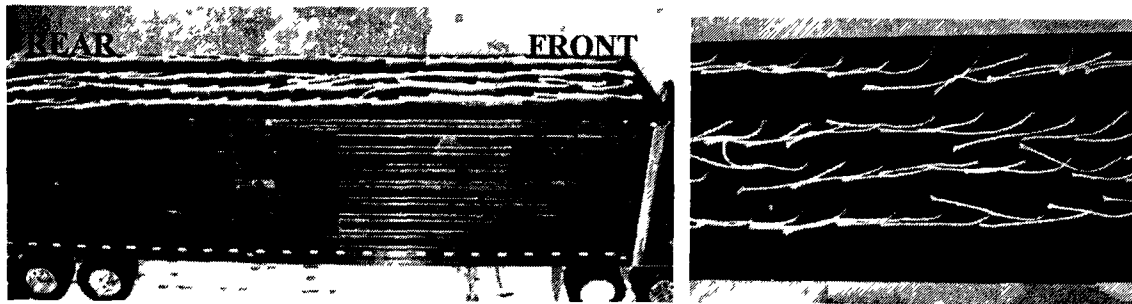
(a) Flow pattern on the top surface of trailer box when using conventional deflector
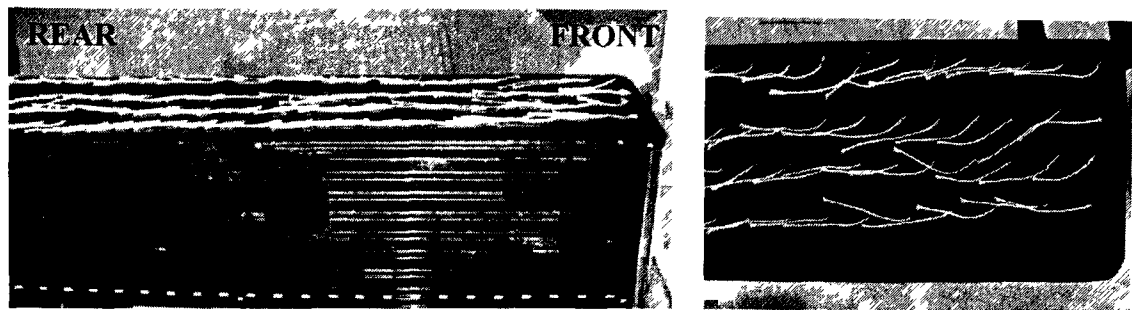
(b) Flow pattern on the top surface of trailer box when using the proposed three concave surfaces deflector
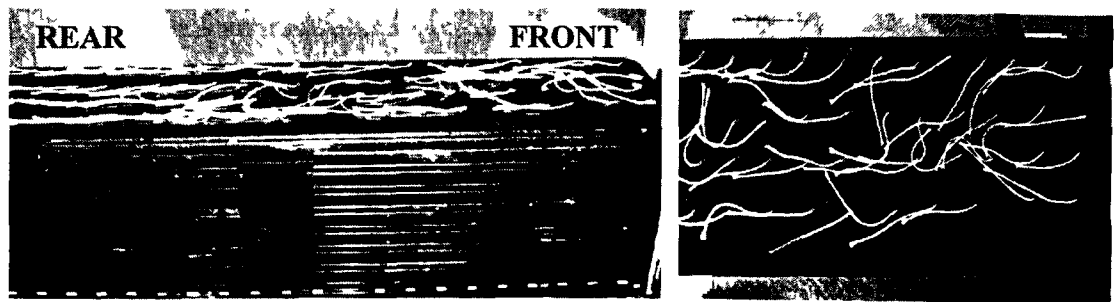
(c) Flow pattern on the top surface of trailer box when using inclined flat surface deflector (30 degree)
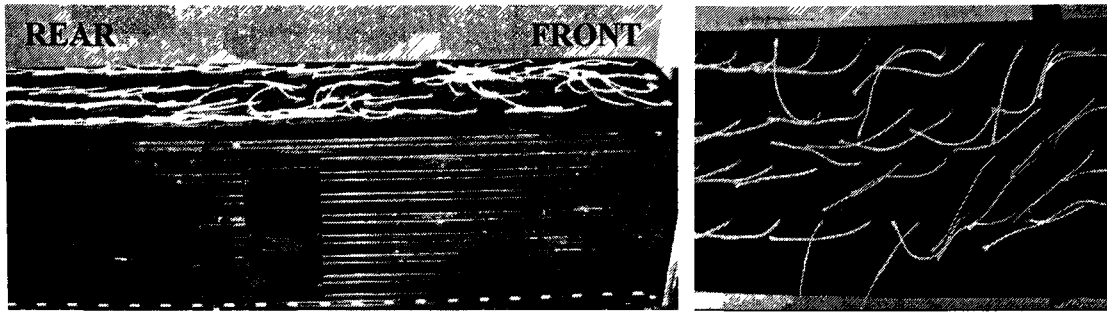
(d) Flow pattern on the top surface of trailer box when using inclined flat surface deflector (45 degree)

Figure 4.1 Flow pattern around truck model when using different deflectors

The air flow around the top surface of the trailer box in Figure 4.1 (a) and Figure 4.1 (b) seems smooth and without any separation or vortex. In Figure 4.1 (c) and Figure 4.1 (d), by using the inclined flat surface deflectors, it can be seen that a vortices forms in the front area of the trailer top surface. The flow characteristics on the side surface of the truck model using all the four different deflectors were also studied. A slight difference was observed among all the cases. It indicated that the change of deflector didn't significant affect the flow around the side surfaces of the truck. Another reason could be, by using such a small-scale truck model, the difference is not obvious to be observed.

4.2 Impact of Friction

The friction between the tires of truck model and the elevated plate could significantly distort the load cell reading for drag. To evaluate such an impact, a piece of wax paper was placed under the model truck tires to minimize friction. An oil sheet was applied to fill the space in the pattern of the tires, to make sure the truck model is able to move freely when the force is applied.

To justify the effectiveness of using wax paper and oil in minimizing the impact of friction between vehicle tires and elevated plate on drag measurement, a series of experiments were conducted on drag measurement by using a simple bluff body with and without wax paper and oil, the results were compared with existing literatures.

34

The experiments were conducted on a circular cylinder with a length of 75cm and diameter of 4.85cm. The cylinder is hollow and with a thickness of 0.5cm, thus, the contact area between the bottom of the cylinder and the wind tunnel floor is reduced close to the contact area between the tires of the truck model and the elevated plate. Thus the experimental results can be applied to the truck model cases. It was mounted on the floor of wind tunnel test section connected to the loadcell system by four strings with angles of α and α', as sketched in Figure 4.2 and Figure 4.3.
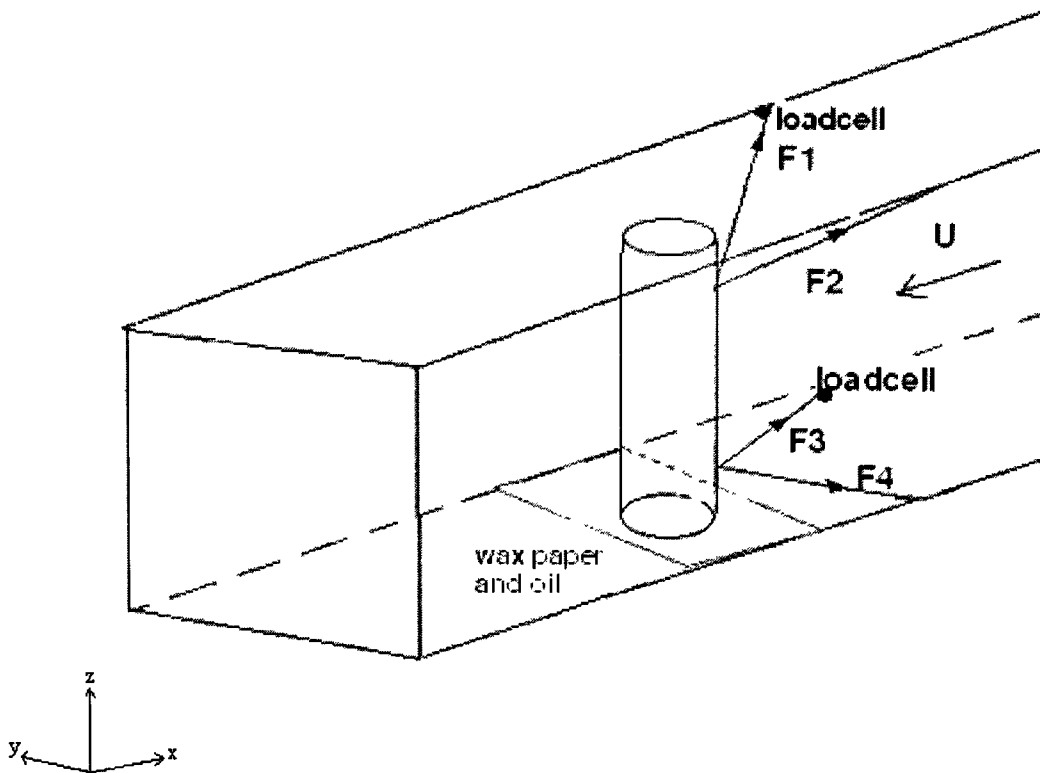
Figure 4.2 Schematic of the experiment setup for drag force measurement on cylinder

Drag fore measurement and calculation procedure

The loadcell was attached to one of the top upstream strings and one of the bottom upstream strings respectively, to measure the net load on those two strings. Due to the symmetric layout of the strings, the drag of the cylinder was therefore determined by the adding of the horizontal streamwise components of the net loads in those two strings multiplied by two, which was calculated below,

As shown in Figure 4.3

α, α , β, β' = geometrical angle of cylinder setup

$F_{D\text{-}TOP}=F_1*\sin\alpha\ \cos\beta$ 　　(along the wind direction)

$F_{D\text{-}BOTTOM}=F_3*\sin\alpha'\cos\beta'$ 　(along the wind direction)

Because F_1 and F_2, F_3 and F_4 are symmetrical in geometry

The total drag force on the cylinder is

$F_{Total}=2F_{D\text{-}TOP}+2F_{D\text{-}BOTTOM}$
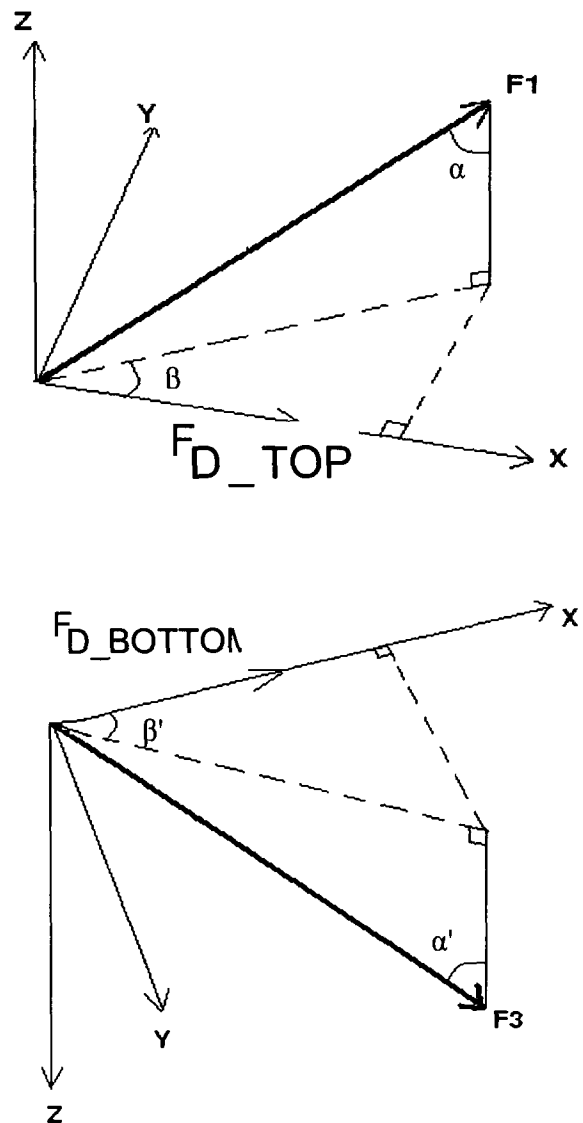
Figure 4.3 Geometric illustrations of strings

The equation used to calculate the drag force is

$F \; (N) = 0.615 F_{load\;cell} \; (mV)$

Which is deduced from the calibration [Strain Sense Ltd., 2007]

$F_D = C_D \; (\rho V^2 \; A/2)$

In this case,

$C_D = 2F_{Total} / \rho \; V^2 \; A$

$Re = VD/\nu$

where V=6m/s, 8m/s, 10m/s, 12m/s

$A = D \times L_{cylinder} = 4.85cm \times 75cm = 363.75cm^2 = 0.0364m^2$

$D = 0.0485m$
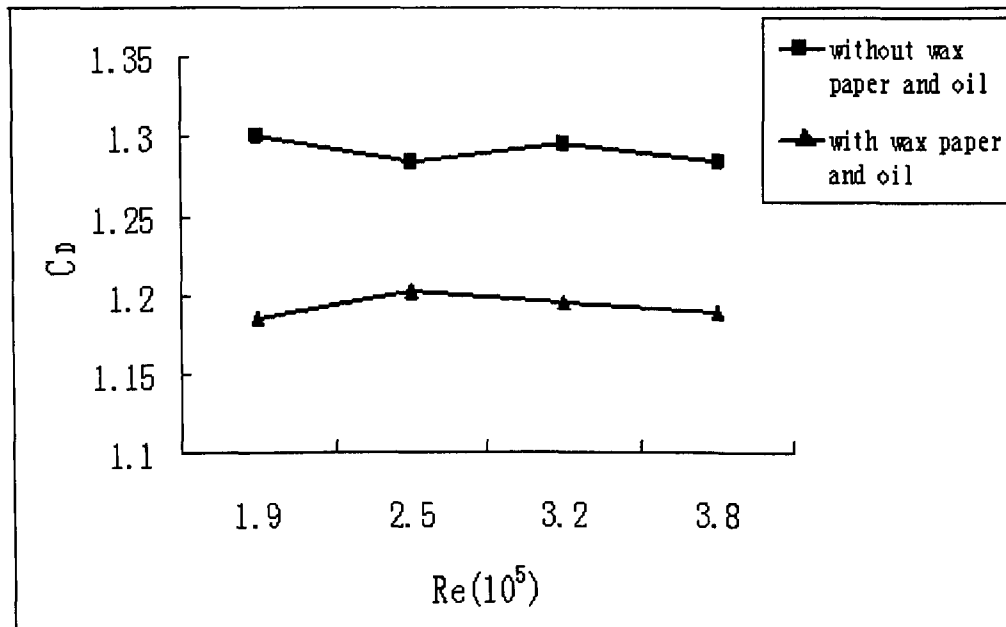
Figure 4.4 Drag coefficients as a function of Reynolds number on friction testing.

Figure 4.4 shows that without placing wax paper and oil between the wind tunnel floor and the cylinder, the drag coefficient is between 1.28 and 1.30. By utilizing the wax paper and oil to reduce the friction, the drag coefficient is deduced to 1.19 to 1.20 at the same range of Reynolds numbers. Most of those points are within a reasonable range compared with the previous studies, which is summarized in Figure 4.5.
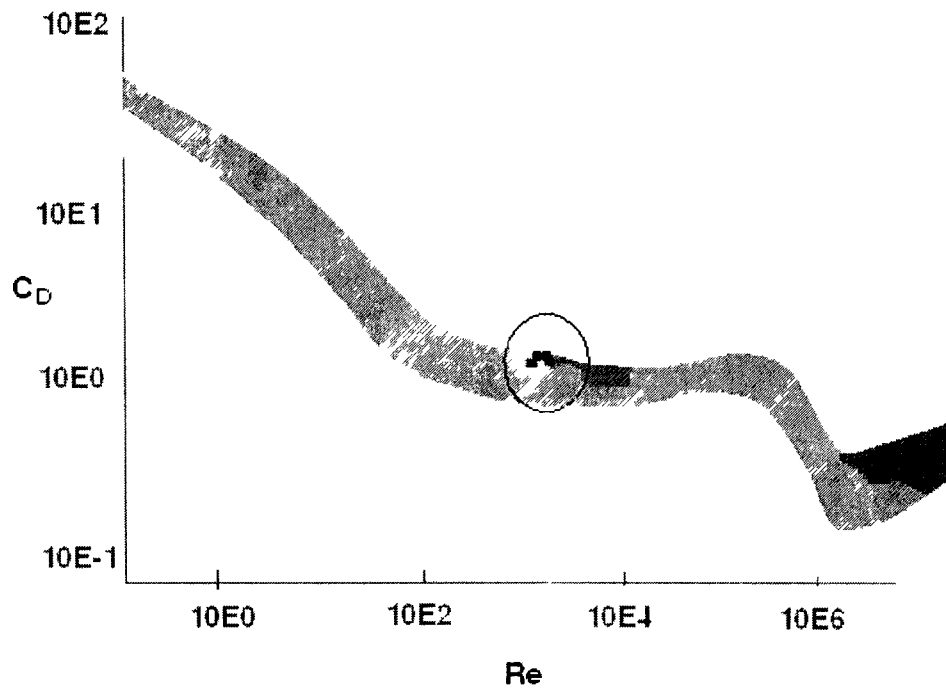
Figure 4.5 Experiment results compared to the standard curve

The standard curve in Figure 4.5 is derived from:

[Yeboah and Rahai, 1997; Lim and Lee, 2004; Schewe, 1983; Sumner, 2004, Golling, 2006; Poulin and Larsen, 2007].

By plotting the present experimental results in Figure 4.4 into the standard curve in Figure 4.5, it is observed that, only one point at Reynolds number 2.5×10^4 is slightly higher than 1.2 (maximum C_D Value from previous study at the same Reynolds number). It can be concluded that the method of using the wax paper and oil to reduce friction suitable. It can be utilized to the truck model case for further investigation.

The test was then repeated for the truck model case The drag of the model truck measured with and without wax paper is presented in Figure 4.6 at 5 different Reynolds numbers.
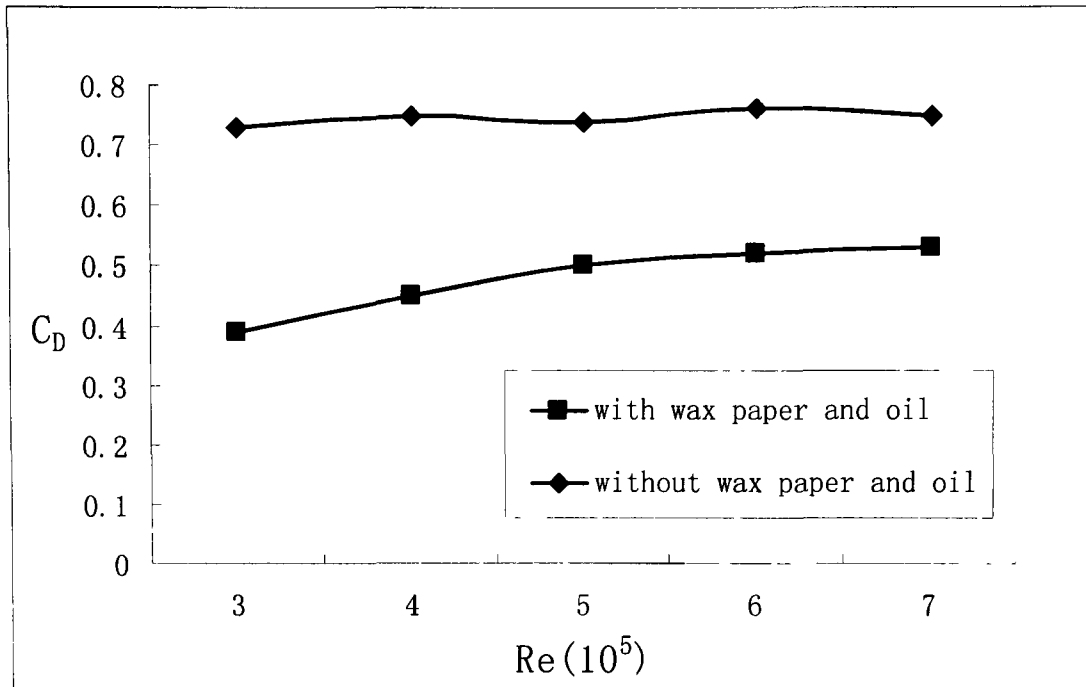
Figure 4.6 Impact of friction on drag measurement (conventional deflector)

From Figure 4.6, it reveals that the friction between the truck model tires and the elevated plate affects the drag measurement results considerably. It can be seen that, drag coefficient is much higher (46% maximum at $Re=3 \times 10^5$) in the absence of the wax paper. As the Reynolds number increases, the difference in drag coefficient between these two cases becomes smaller, at the maximum studied velocity of 14m/s ($Re=7 \times 10^5$), the drag coefficient of the case without wax paper is about 30% greater than that of the case with wax paper, which indicates the effect of friction between the model truck tires and the elevated plate reduces at higher Reynolds number. After minimizing the impact of friction, the drag coefficient obtained from this study is in the range of 0.38 ~ 0.54, which agrees with the existing data from previous work of Berta and Tacca [1980], and Cooper [2003]: The drag coefficient of the truck with a streamlined cab at a zero yaw angle and a Reynolds number of at half a million is in the range of 0.30-0.55.

4.3 Drag Force Measurements

A series of tests were carried out under smooth flow condition (Tu<0.55%), at nominal mean flow velocities of 6m/s, 8m/s, 10m/s, 12m/s and 14m/s, which correspond to Re=3×10^5, 4×10^5, 5×10^5, 6×10^5, 7×10^5, respectively. The drag coefficient of the model truck measured using the proposed concave deflector, conventional deflector and without deflector is presented in Figure 4.7.
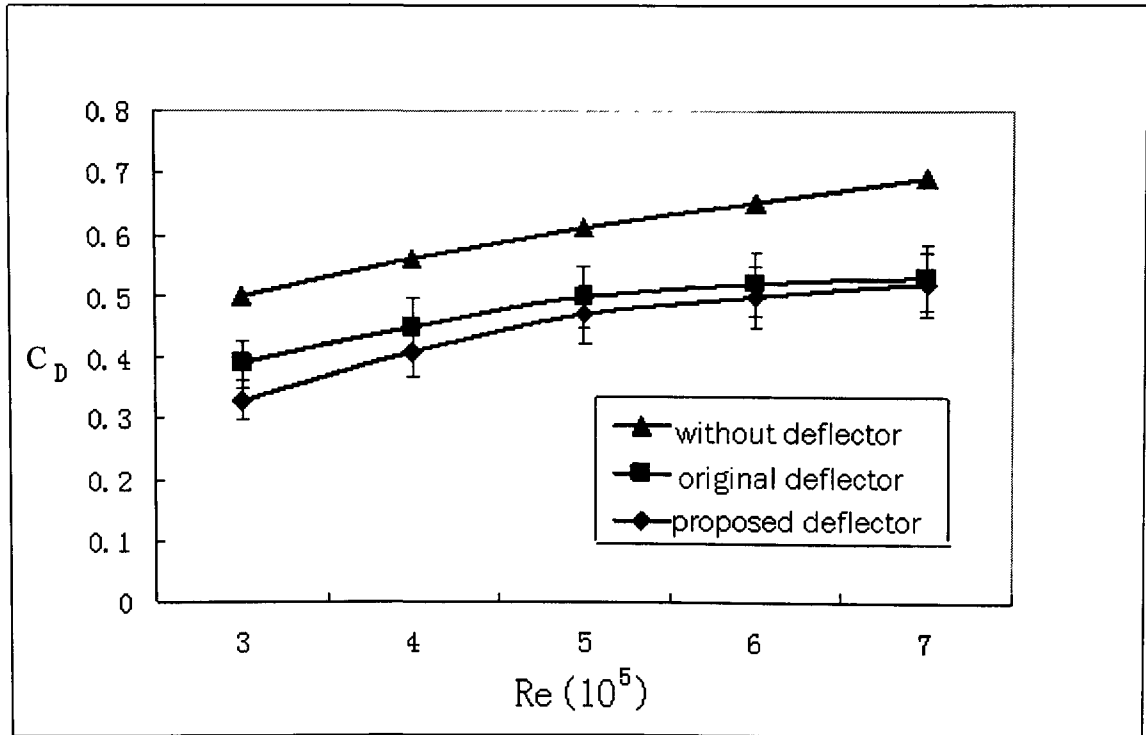
Figure 4.7 Drag coefficients of model truck with different air deflectors under
smooth flow condition

From Figure 4.7, by comparing the two C_D-Re curves of the proposed deflector and the conventional deflector, it can be seen that under smooth flow condition, when the Reynolds number is relatively low (Re=3×10^5), the drag coefficient of the proposed concave deflector is approximately 24% smaller than that of the conventional one. The C_D difference between them becomes less obvious when the Reynolds number increases. Both of these two curves show the same tendency, i.e., as the Reynolds number goes up, the increasing slope of C_D becomes smaller. For the drag of a model truck without a

deflector, results show that the drag coefficient is relatively higher than that with the conventional convex deflector (29% maximum).

4.4 Impact of Yaw Angle

A zero yaw angle corrsponds to driving in still wind, which never occurs in reality and can not provide sufficient indication of aerodynamic characteristics in real operation. Thus, the effect of yaw angle on drag coefficient should be taken into consideration in wind tunnel study. In this series of test, drag measurement for the tractor-trailer model with different air deflectors in yawed wind was conducted. Due to the limited width of the wind tunnel, a yaw angle range of -5° to +5° was investigated.
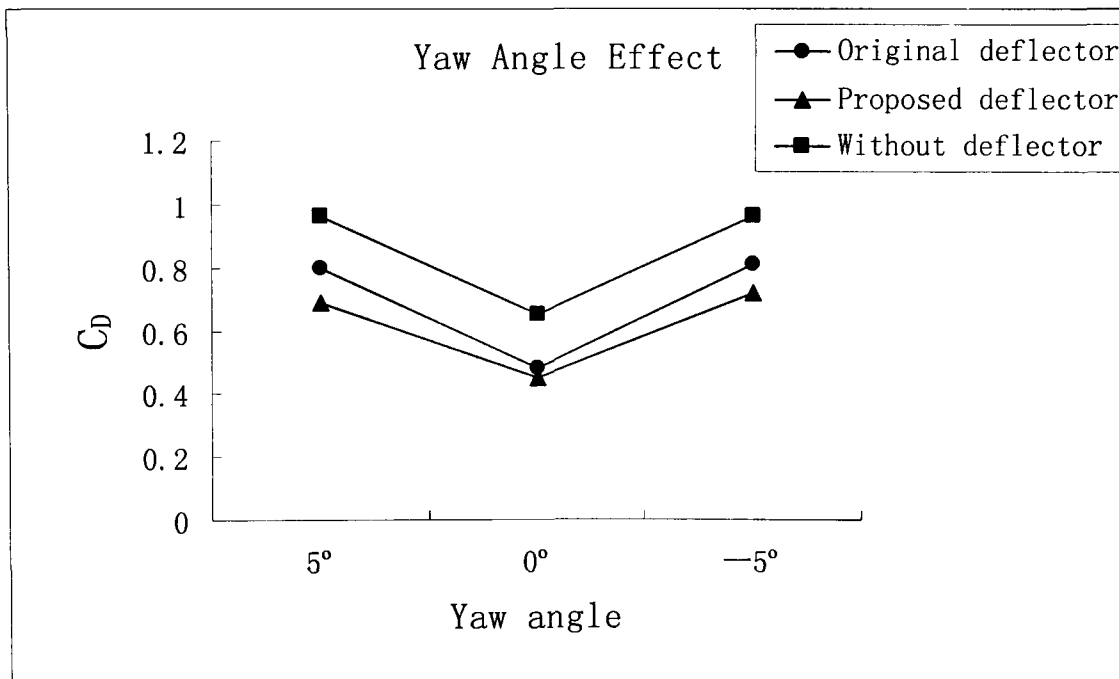
Figure 4.8 Influence of Deflector Shape versus Yaw Angle (Re=6×10⁵)

From Figure 4.8, a considerable increase in C_D with increasing yaw angle is observed in all three cases tested. The C_D difference between the proposed deflector case and the original deflector case becomes larger at ±5° yaw angle, which indicates that in a yaw wind condition, the proposed concave deflector can reduce the drag force applied on the truck model more significantly. More experiments need to be carried out in larger yaw angle conditions to confirm this finding.

4.5 Wake Bubble

It is known from Yang's study [2008] that details of vehicle shape affect the aerodynamic characteristics of the wake area. As a further research, the characteristics of the wake bubble are investigated by changing different air deflectors. The first series of experiments were carried out in the centre plane behind the truck model.

Considering the importance of the recirculation length in the study of wake characteristic, First of all, how to deduce the recirculation length is illustrated in Figure 4.9.
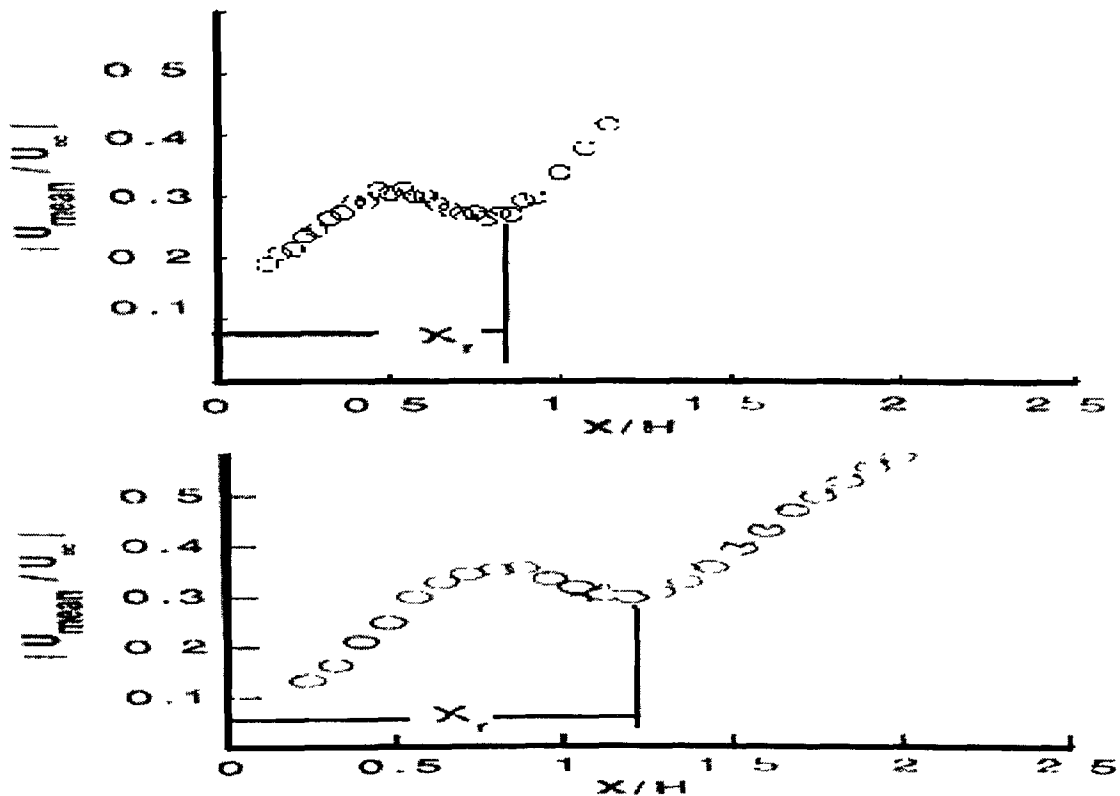
Figure 4.9 Near-wake time-averaged velocity distribution and recirculation length in

each horizontal line at the vertical central plane [Duell and George, 1993]

As shown in Figure 4.9, U_m is local mean velocity, U_∞ is the free stream velocity. The recirculation length is the largest X_r. deduced from the distance between the model rear end and the stagnation point, where the first derivative of the velocity with respect to streamwise distance x is zero and the second derivative is positive. In other words, X_r is

the distance from the model rear end to the point where the slope of velocity profile in the streamwise direction is 0 and curvature is upward (positive).

In Figures 4.10 (a)-(c), three collections of stagnation points along the horizontal lines in the measuring grid are shown, the recirculation length and the bubble shape (consisted of X_r in each horizontal lines) obtained by using different air deflectors are illustrated.
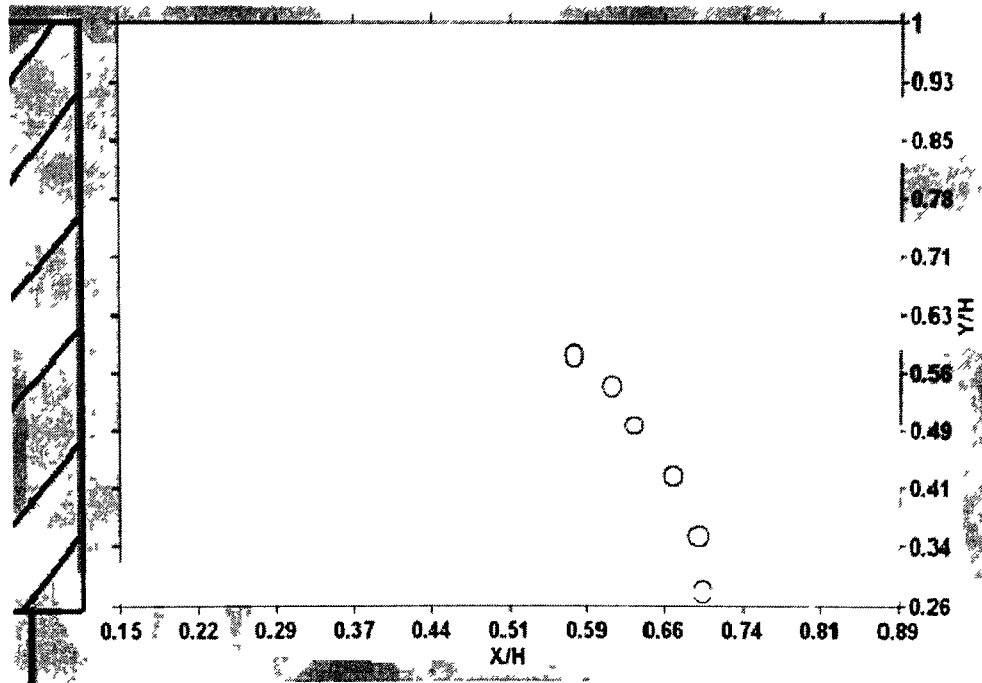
Figure 4.10 (a) Bubble shape of the truck model using original deflector in the wake at Re=5×10^5
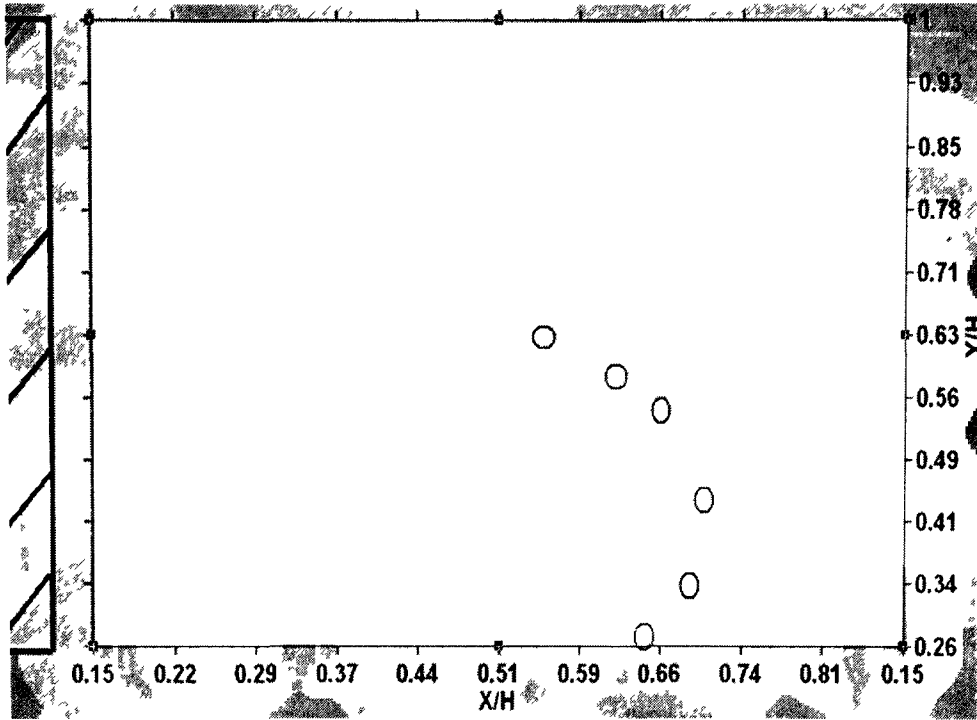
Figure 4.10 (b) Bubble shape of the truck model using proposed deflector in the wake at Re=5×10^5
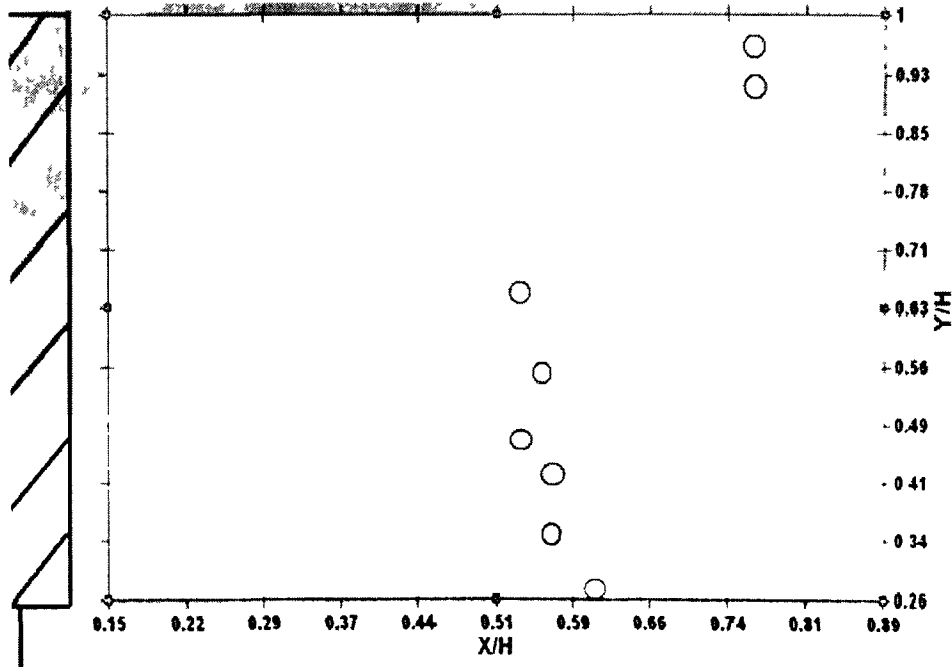
Figure 4.10 (c) Bubble shape of the truck model without deflector in the wake at Re=5×10^5

In term of recirculation length, compare Figure 4.10 (a) and Figure 4.10 (b), the conventional deflector and the proposed one yield 0.71 versus 0.73, which means the later case has a relatively larger (longer) near wake region than the former one. The reason may caused by the delayed flow separation around the frontal area of the truck model by using the proposed concave deflector.

Concerning the shape of the bubbles, connecting the lower 6 points in Figure 4.10 (b), a "two-dimensional bubble" appears which is more rounded and circular comparing to the one form in Figure 4.10 (a). In Figure 4.10 (c), although mathematically the stagnation points in some horizontal grid lines can still be determined, but by connecting these points, it really doesn't look like a "real bubble", it is much blunt. Those two points appear in the upper region in Figure 4.10 (c) may be caused by unexpected vortex and need to be further investigated.

To deduce and understand the relationship between the bubble shapes and drag force, some relevant previous research work was studied. According to Roy and Srinivasan's work [2000], CFD was used to obtain the external flow around the truck models of different frontal shape; an on-road speed of 60 mph was simulated in that study. The results show that, the details of flow vector behind a truck model with rectangular front (as in our case: truck model without deflector) showed strong recirculation and resultant source of pressure drop, which indicates a larger drag force. Less flow vortices are shown behind a truck model with the rounded frontal shape (as the conventional deflector in our case). It indicates a smaller drag force, which leads to over 28% drag reduction.

Comparing the results in Figures 4.10 (a)-(c) to Roy and Srinivasan's work, there is less vortex forms to disturb the bubble shape in the wake area by using the proposed deflector in Figure 4.10 (b), thus, leads to a less drag force. On the other hand, in the case of truck model without deflector, more vortices behind the truck model form to disturb the bubble shape (Figure 4.10 (c)), which leads to a larger drag force. To sum up, the proposed deflector leads to less drag force comparing to the conventional one, and the truck model

without deflector leads to the largest drag force. These conclusions are consistent with the results of drag force measurements shown in the previous sections.

Then, experiments were repeated in side planes (Z=±1 in, Z=±2 in) by using the original deflector and the proposed deflector respectively, to show 3D feature of the wake bubble. The results are shown in Figure 4.11 and Figure 4.12. A sketch of three-dimensional bubble is shown in Figure 4.13.

(a) Z= +1 in   (b) Z= − 1 in
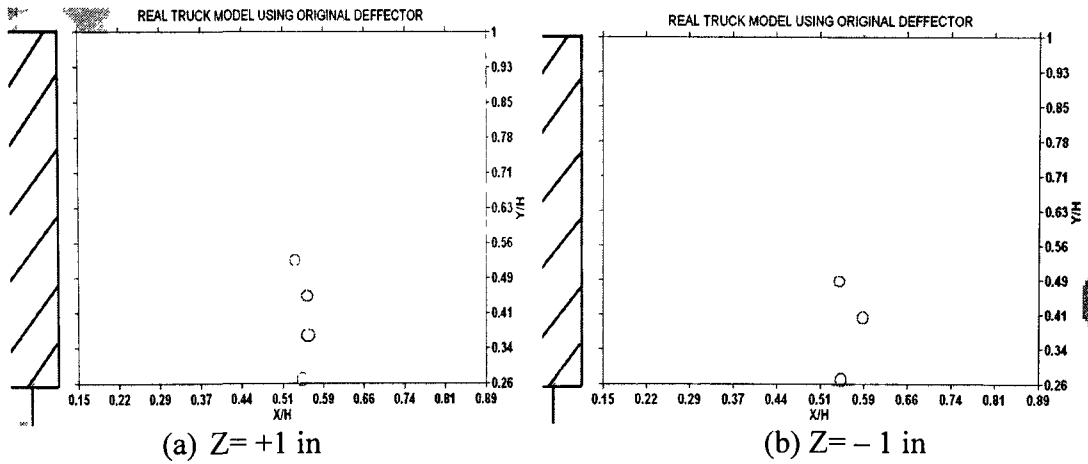
Figure 4.11 Wake bubble in the side plane by using the original deflector.

(a) Z= +1 in   (b) Z= − 1 in
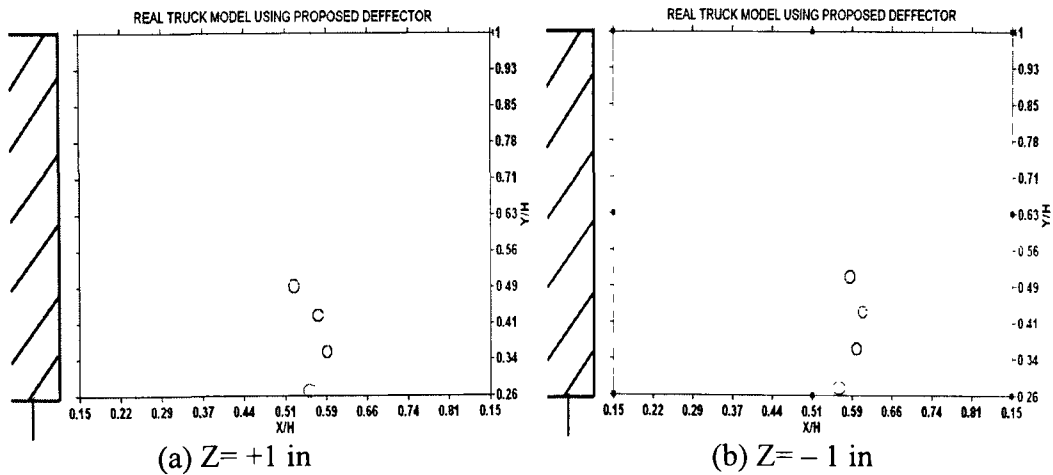
Figure 4.12 Wake bubble in the side plane by using the proposed deflector.

Z=+1in   Z=0   Z=-1in
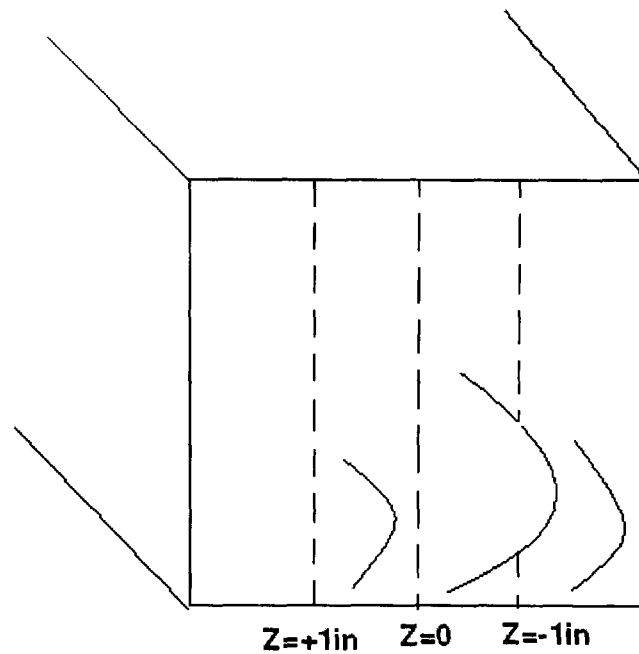
Figure 4.13: The sketch of a three-dimensional bubble

The results in Figures 4.11-4.12 show that, the normalized recirculation length X_r/H in the side planes by using the original deflector is 0.58/0.59 (+1 in/ − 1 in); the normalized recirculation length in the side planes by using the proposed deflector is 0.60/0.62 (+1 in/ − 1 in). These results are consistent with the results in the central plane: the recirculation length by using the proposed deflector is greater than that by using the original deflector.

Based on the sketch of a three-dimensional bubble (Figure 4.13), to c oncluded, the proposed deflector seems to have a larger and more streamlined bubble region, which indicates less drag force applied on the truck model corresponding to the results of C_D measurements obtained by using the proposed deflector and the original deflector.

There is no wake bubble appears in the ±2 inch (0.052m) side planes in both cases. The maximum discrepancy between the left plane and the right plane in this series of experiments is 0.02 (3.2%), which is acceptable.

47

Chapter 5 Conclusions and Recommendations

In this study, a newly designed air deflector with the shape of three concave surfaces was proposed, a series of wind tunnel experiments were carried out to evaluate the impact of air deflector shape on the aerodynamic performance of a tractor-trailer. The range of Reynolds number studied in this project is from 3×10^5 to 7×10^5 The main conclusions and recommendations are detailed as follows:

5.1 Conclusions

- Firstly, to evaluate the method of friction reduction, the drag force measurement by using a circular cylinder was carried out. The results showed that by utilizing the wax paper and oil to reduce the friction, the drag coefficient of the cylinder can be reduced in reasonable range compared to the previous study, which means the method of friction reduction used in this experiment is suitable.

- After placing wax paper and oil sheet between the tires and the elevated plate to reduce drag force, the experimental results of drag force measurement by using the truck model with different deflectors showed:

1) Reynolds number effect:

   Under smooth flow condition (Tu<0.55%), when the Reynolds number is relatively low (Re=3×10^5), the drag coefficient of the proposed concave deflector is approximately 24% smaller than that of the conventional one; when the Reynolds number increases, the C_D difference between these two cases becomes smaller. The drag coefficient by using the truck model without deflector is much higher than the other two cases regardless the change of Reynolds number in this study.

2) Yaw angle effect:

   In a yawing wind condition (yaw angle = ±5 °), for the studied Reynolds number range, the proposed concave deflector can reduce more drag force applied on the truck model than the conventional convex deflector.

48

- Concerning the characteristics in the wake area, the proposed deflector has a relatively larger (longer and more streamlined) near wake region than the conventional deflector in terms of recirculation length. In terms of bubble shape, the experimental results indicate that the proposed deflector leads to less drag force compared to the conventional one, and the truck model without deflector has the largest drag force. These conclusions are consistent with the results of drag force measurements.

5.2 Recommendations

- The maximum Reynolds number covered in this study is 7×10^5, which is similar to that obtained by Duell and George [1993, 1999] and Yang [2008]'s study. In the real scenario Re $= 7 \times 10^5$ corresponds to 2.1 km/h, which is relatively low and needs to be extrapolated to higher order for reality use. Based on Wiedeman's work in 1989, Reynolds number can be extrapolated from 4×10^5 to 7×10^5 by using different turbulence generating screens, which means the effective Reynolds number can be increased by increasing turbulence level. This method is generally applicable in wind tunnel experiments. For this project, because the deflector is a widely used drag reduction device in reality, and it has a huge potential for fuel saving and economy return, the future work should be focused on how to extrapolate to higher Reynolds numbers to ensure the results obtained in these low Reynolds number studies are valid in real life.

- From Watkins' (1990) study, he found that tunnel measurements obtained in smooth flow would consistently over predict on-road drag coefficient reductions caused from add on aerodynamics devices, especially at high yaw angles. For those add-on deflectors, which depend on a stable wake to shield the load, turbulence simulation should be investigated to correct the discrepancy between the tunnel and on-road results. But most studies in this area were conducted in extremely low-turbulence wind tunnel (turbulence intensity <1%). which is contrary to situations in reality; the turbulence environment experienced by ground vehicles is currently not well understood. So it is recommended that more experiments be carried out in turbulent

flow conditions, the effect of turbulence intensity and integral length scale should be further studied.

- For the flow visualization work, tuft wool was used in this project. To know more details about how the airflow goes around the surface of truck model by using different shape deflectors, thus predict the drag force formed in that area, CFD simulation is suggested in future studies.

- The effect of larger yaw angle on C_D needs to be conducted to investigate the aerodynamic performance of different shape deflectors in cross-wind conditions.

- The most significant contribution in this project is

a) Bring new idea to the field of deflector design.

b) Provide information in an early phase of aerodynamic characteristics investigation by using the proposed deflector.

REFERENCES

Ahmed, S. R., Ramm, G., and Faltin, G., "Some salient features of the time-averaged ground vehicle wake", SAE paper 840300, 1984.

Baker, C.J. and Brokie, N.J., "Wind tunnel tests to obtain train aerodynamic drag coefficients: Reynolds number and ground simulation effects", Journal of Wind Engineering and Industrial Aerodynamics, 38(1991)23-28, 1991.

Barlow, J. B. Rae, W. H and Alan Pope Jr., "Low-speed wind tunnel testing", Third edition, Wiley Interscience, 1999.

Berta, C. and Bonis, B., "On Shape Experimental Research of Ideal Aerodynamic Characteristics for Industrial Vehicles", SAE paper No. 801402, Society of Automotive Engineer, Warrendale, Pa., 1980.

Berta, C. and Tacca, T., "Aerodynamic Study on Vehicle Shape With the "Panel Method"· An Effort to Calculate the Influence of Shape Characteristics on Aerodynamic Performance", SAE paper 801401, 1980.

Bischof, G., Bratscjitsch, E., Haas, A., Kaltenhauser, A., and Ullrich, F., "On-road determination of aerodynamic drag improvements", Journal of Automobile Engineering, 2004.

Carlino, G., "First investigation of car front lift in the present of large scale longitudinal vortices", ECARA - Unsteady Aerodynamics Committee Meeting, Emmen, 2004.

Cooper, K.R., "Truck Aerodynamics Reborn-Lessons from the Past" SAE paper No. 2003-01-3376, 2003.

Du, G.S., Li, L., and Zhou, L.D., "Characteristics of Wind Deflector for Reducing Aerodynamics Drag of Van-body Truck" Journal of Hydrodynamics. Ser.B, 4-58, 2003.

Duell, E. G and George, A. R., "Measurements in the unsteady near wake of ground vehicle bodies", SAE paper 930298, 1993.

Duell, E. G and George, A. R., "Experimental study of a ground vehicle body unsteady near wake", SAE paper 990812, 1999.

Engar, R.J., "Advanced Aerodynamic Devices to Improve the Performance, Economics,Handling and Safety of Heavy Vehicles", SAE paper 2001-01-2072, 2001.

Garry, K.P., "Wind tunnel tests on the influence of fixed ground board length on the aerodynamic characteristics of simple commercial vehicle models", Journal of Wind Engineering and Industrial Aerodynamics. v38, n1, p 1-10, 1991.

Golling,B., "Experimental investigations of separating boundary-layer flow from circular cylinder at Reynolds numbers from 105 up to 107" German Aerospace Centre. 2006.

Gross, D.S., and Sekscienski, W.S., "Some Problem Concerning Wind Tunnel Testing of Automotive Vehicles", SAE paper 660385. 1966.

Harris, H.T., "Fuel saving through aerodynamic drag reduction of trucks" The South African Mechanical Engineer, Vol 30. June 1980.

Hucho, W.H., "Aerodynamics of Road Vehicle: From Fluid Mechanics to Vehicle Engineering" Fourth edition, SAE International, 1998.

Lanser, W.R., Ross, J.C., and Kaufman, A.E., "Aerodynamic Performance of a Drag Reduction Device on a Full-Scale Tractor/Trailer", SAE paper No. 912125, 1991.

Lim, H.C., and Lee, S.J., "Flow control of a circular cylinder with O-rings", Fluid Dynamics Research, 2004.

Losito, V and Nicola C.D, "An improved method of computing the wake effects on aerodynamic characteristics of road vehicle", International Journal of Vehicle Design, special publication sp3, 1983.

Mason, W. T., JR., and Beebe, P. S., "The Drag Related Flow Field Characteristics of Trucks and Buses", AICHE Symposium Series, p 45-90, 1978.

McLandress, A.S., Wiese, W., Turney, J. and Loczi J., "A Two-Dimensional External Aerodynamics Tool(EAT) for Simulating Airflow around Tractor-Trailer Combination" SAE paper 2001-01-2743, 2001.

Monkewitz, M., and Muller, J., "Measuring of long Truck Models in a Wind Tunnel with External Balance" SAE paper No, 2008-01-1202, 2008.

National Research Council (NRC), Canada, Annual Report, 2006.

Patel, P. and Vijayakumar, S., "External Flow Analysis over a Car to Study the influence of Different Body Profiles Using CFD", SAE paper 2001-01-3085. 2001.

Poulin,S. and Larsen, A., "Drag loading of circular cylinders inclined in the along-wind direction." COWI A/S, Parallelevej 2, 2800 Lyngby, Demark. 2007.

Roy, S., and Srinivasan, P., "External Flow Analysis of a Truck for Drag Reduction", SAE paper 2000-01-3500, 2000.

Schewe,G., "On the force fluctuations acting on a circular cylinder in cross flow from subcritical up to transcritical Reynolds numbers", DFVLR-Institut fiir Aeroelastik (AVA),1983.

Schoon, R., and Pan, F P., "Practical Devices for Heavy Truck Aerodynamic Drag Reduction", SAE paper 2007-01-1781, 2007 (Original published as SAE 2006-01-3531 in 2006).

Schoon, R., "On-Road Evaluation of Devices to Reduce Heavy Truck Aerodynamic Drag" SAE paper 2007-01-4294, 2007.

Storms, B.L., Satan, D.R., Heineck, J.T., and Walker, S.M., "A Study of Reynolds Number Effects and Drag Reduction Concepts on a Generic Tractor-Trailer" 34th AIAA Fluid Dynamics Conference and Exhibit. AIAA-2004-2251, 2004.

Strain Sense Ltd., 2007

Sumner, D., Heseltine, J.L., and Dansereau, O.J.P., "Wake structure of a finite circular cylinder of small aspect ratio" Experiments in Fluids 37(2004)720-730, 2004.

Surcel, M.D., Michaelsen, J. and Provencher, Y., "Track-test Evaluation of Aerodynamic Drag Reducing Measures for Class 8 Tractor-trailers", SAE paper 08CV-0068, 2008.

Vexler, S.F., and Katz, J., "Full-Scale, On-Road Study of the Effect of Automobile Shape on Its Aerodynamic Characteristics and Comparison with Small-Scale Wind Tunnel Results", SAE paper 850287, 1985.

Villanueva, J. J., "Visualization, imaging, and image processing" Proceedings of the Second IASTED International Conference in USA, 2002.

Wayne, M.J., "Evaluation of On-Road Results from a Test Fleet of Heavy-Duty Trucks" California Air Resources Board Research Division. April, 2007

Watkins, S., "Wind-Tunnel Modeling of Vehicle Aerodynamics: With Emphasis on Turbulent Wind Effects on Commercial Vehicle Drag", PhD Thesis, Mech Eng Department, RMIT, Melbourne, Australia. 1990.

Wiedemann, J., "Turbulence manipulation to increase effective Reynolds numbers in vehicle aerodynamics", v27, AIAA journal, p 763-769, 1989.

Wood, R. M. and Bauer, S. X., "Simple and Low-Cost Aerodynamic Drag Reduction Devices for Tractor-Trailer Trucks", SAE paper 2003-01-3377, 2003.

Wordley, S., and Saunders, J., "On-road Turbulence", SAE paper 2008-01-0475, 2008.

Yang, D.Q., "Wind Tunnel Study on the Wake Bubble of Model Truck" Mater's thesis. Department of Mechanical, Automotive and Materials Engineering. University of Windsor, 2008.

Yeboah, E.N. and Rahai, H.R. "The Effects of External Turbulence on Mean Pressure Distribution, Drag Coefficient and Wake Characteristics of Smooth Cylinders" ASME Fluids Engineering Division Summer Meeting, 1997

http://www.macsradiator.com/browseproducts/Kenworth--Charge-Air-Coolers.HTML

Appendix A: Hotwire System

This appendix is comprised of 3 sections. In section A.1, detailed calibration instructions for the 1-D hot-wire probe and an example are presented. In sections A.2, a MATLAB program is developed to process the collected data. In A.3, 3 traverse programs are demonstrated.

A.1 Calibration Procedure Instructions and Example

The hot-wire probe was calibrated before each test to establish the relationship between the voltage output from the hot-wire anemometer and the flow velocity. The calibration system consists of a calibration module to be placed in the frame and a separate flow unit connected to the calibration module via cable. The system operates from a pressurized air supply and creates a free jet, where the probes are placed during calibration.

The calibration process consists of two steps: i) A velocity calibration to establish the relationship between the hot-wire voltage output and the given flow velocity; and ii) A yaw angle calibration to identify the dependence of the hot-wire voltage output on the relative position of the hot-wire sensor to the instantaneous flow vector. Because a 1D probe was utilized, no yaw angle calibration was needed in this series of Experiment.

It is assumed that the data acquisition board and the StreamWare® software are installed before this calibration.

The following steps must be taken to achieve the velocity calibrations of the I-D hot-wire probe.

1) Connect the PC and the StreamLine® frame to the power line with the power switched off.
2) Connect the PC serial communication port (COM1) to the Serial Interface connector on the rear of the StreamLine® frame via the Null Modem cable.
3) Connect Analog Output connectors No. 1 and No. 2 on the back panel of the Frame to the SCB-68 shielded connector block channel no. 0 and channel no. 1, respectively,

with two 50 ohm BNC cables. The connector block is connected, in turn, to the A/D board in the PC via a 68-pin parallel cable.

4) Connect the two 4m probe cables with 55H24 probe support and 1-D probe to the probe connector on the CTA Module front plate.

5) Secure the 55H24 probe support onto the mounting tube with the in-house steel collar.

6) Connect the temperature probe (thermistor) to the frame via its 4m cable and place it in the vicinity of the 1-D probe.

7) Place the probe inside the potential core region of the jet formed by the nozzle

8) Switch on both the PC and the Streamline® frame and open up the StreamWare® software.

9) Following the steps listed in Streamline®, Installation and User's Guide [2002], carry out the system configuration which includes the overheat adjustment, square wave test and setup of the parameters for signal conditioning.

10) Start the velocity calibration process in StreamWare® software.

11) Open up the EXCEL file "velocity calibration"

12) Record the atmospheric pressure and room temperature into "velocity calibration" to obtain the air density at the time of calibration.

13) Select Velocity from the Setup menu. The calibration and correction factors for your specific Calibrator are now loaded into the StreamWare software for use in the velocity calculation. This is indicated by the message box "Loading EProm data" When finished, the Velocity Range dialog box opens.

14) Enter 1 m/s as min. and 20 m/s as max velocity and 10 calibration points.

15) Select Apply temperature correction and Apply signal conditioner settings. This gives you the best accuracy, if the temperature changes during the calibration. Deselect the Apply temperature loading. This is only relevant, when you have a project with temperature correction.

16) Select OK. The dialog box closes and you are prompted to install the proper Nozzle. If correct, select Yes. The Select point dialog box opens.

17) Choose All and OK. The (55P11) Calibration dialog box opens.

The figures showed below illustrate the next few steps of calibration procedure.
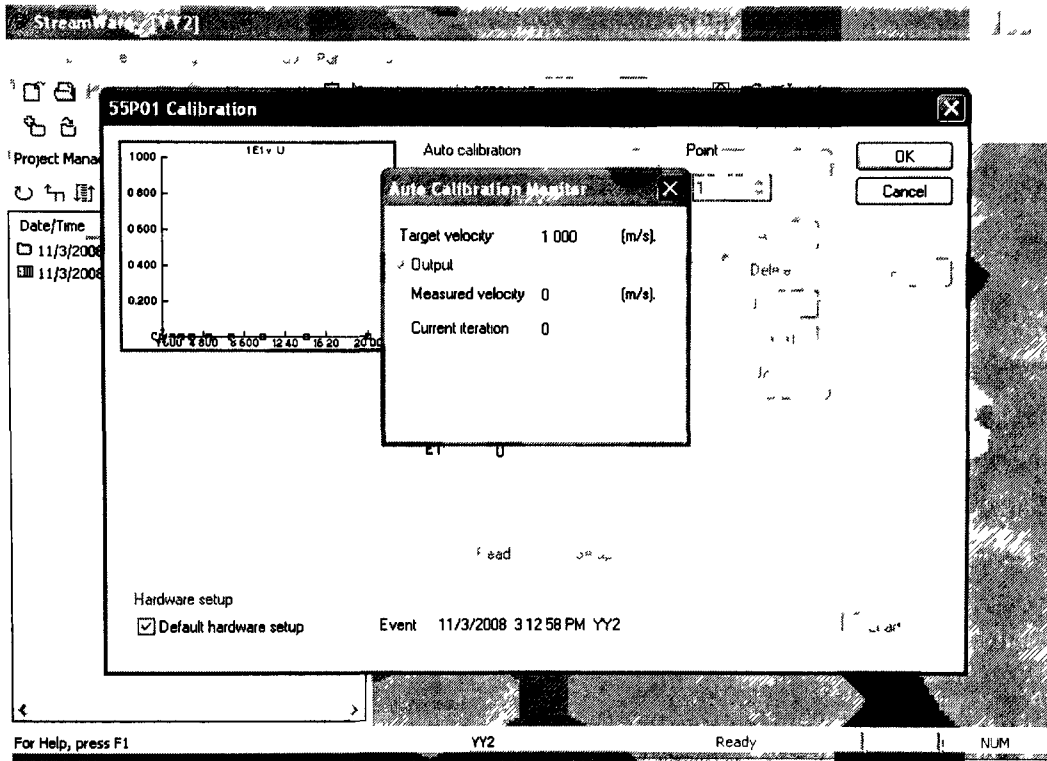
Figure A1 Auto calibration: minimum velocity
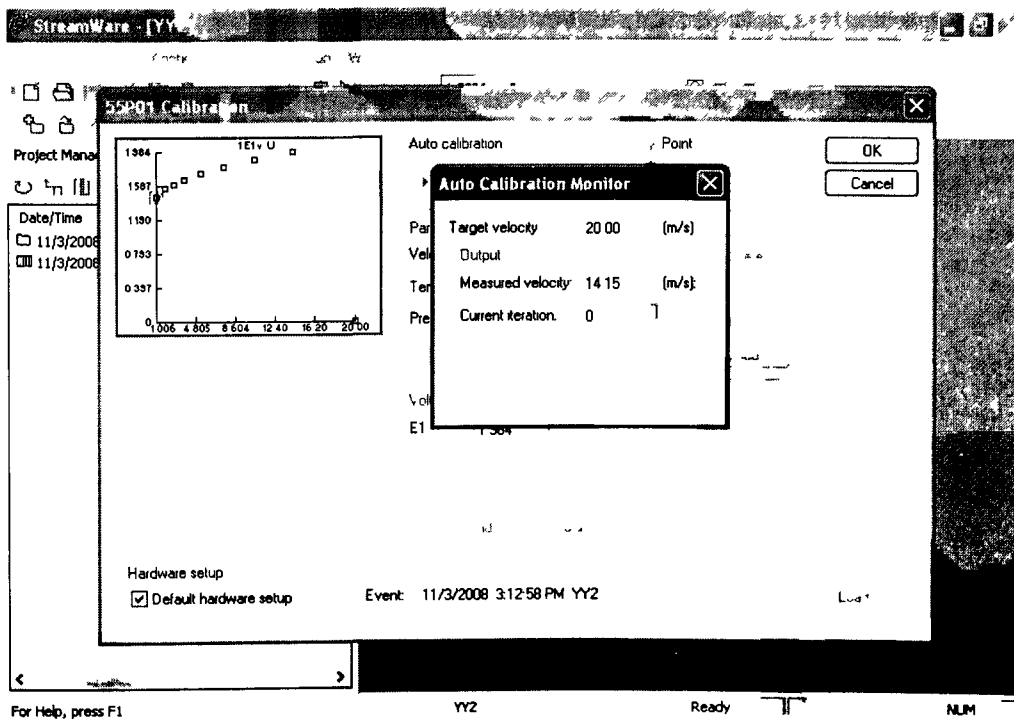
Figure A2 Auto calibration: maximum velocity
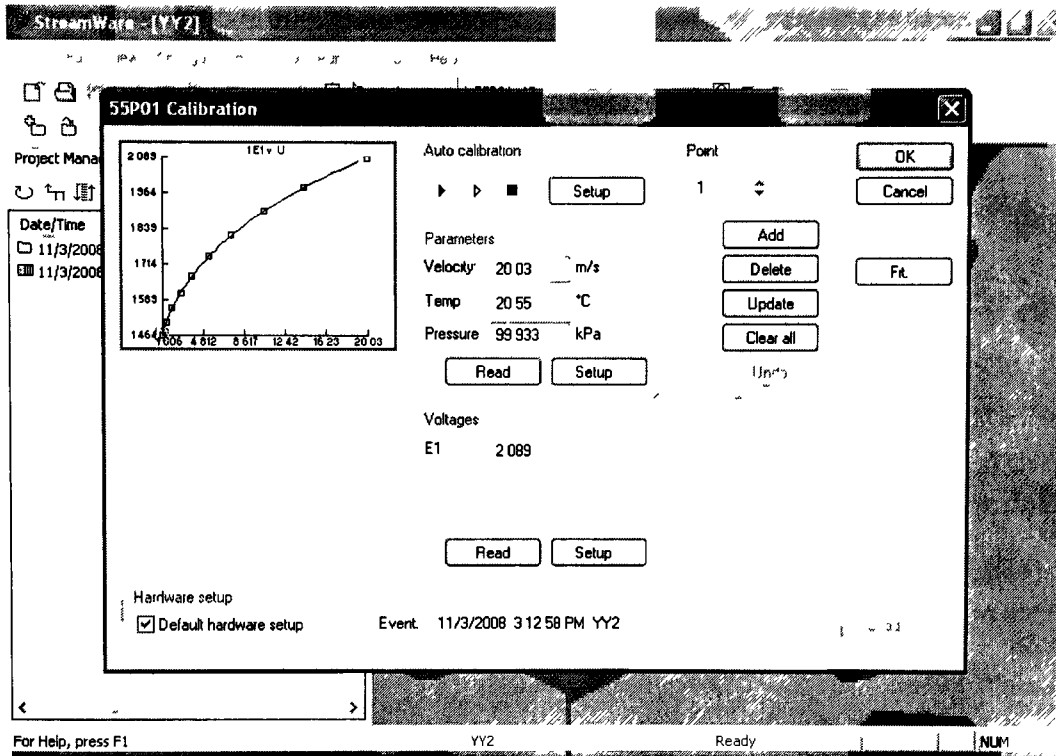
FigureA3 Results of auto calibration.
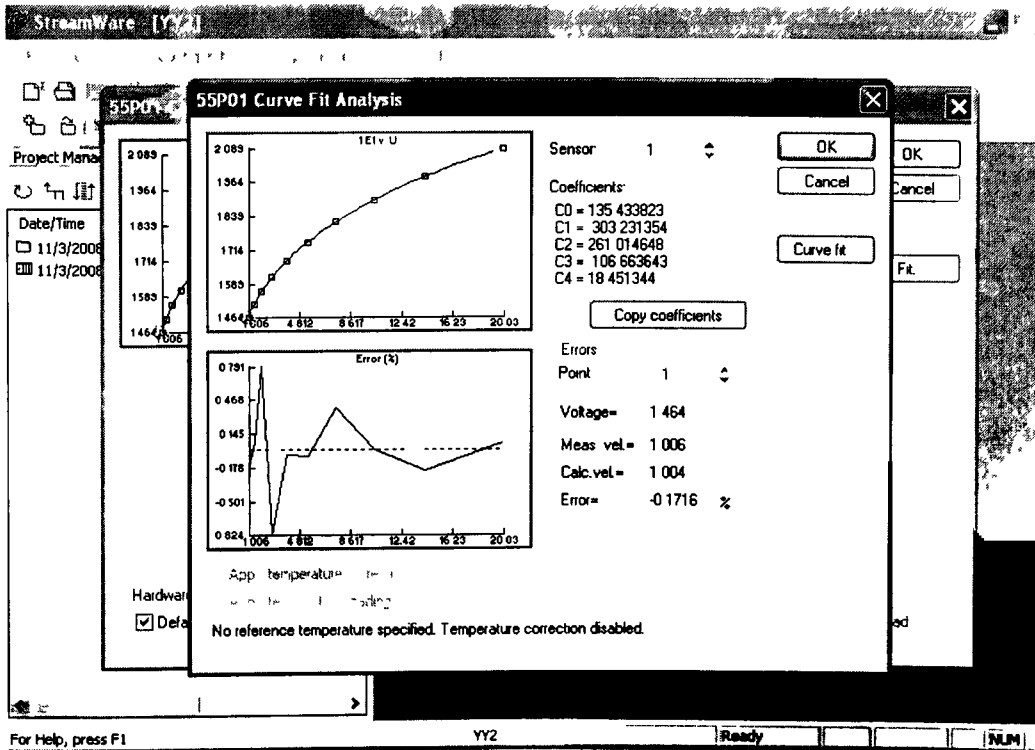
Figure A4 Error of auto calibration
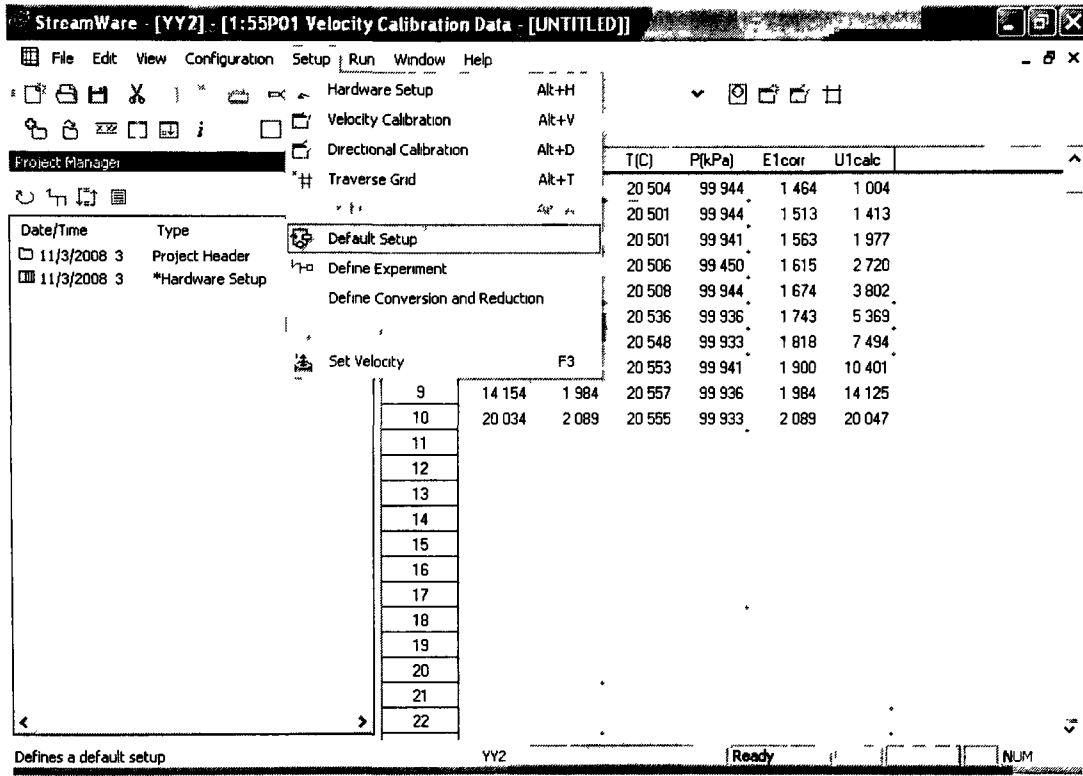
Figure A5 Default Setup
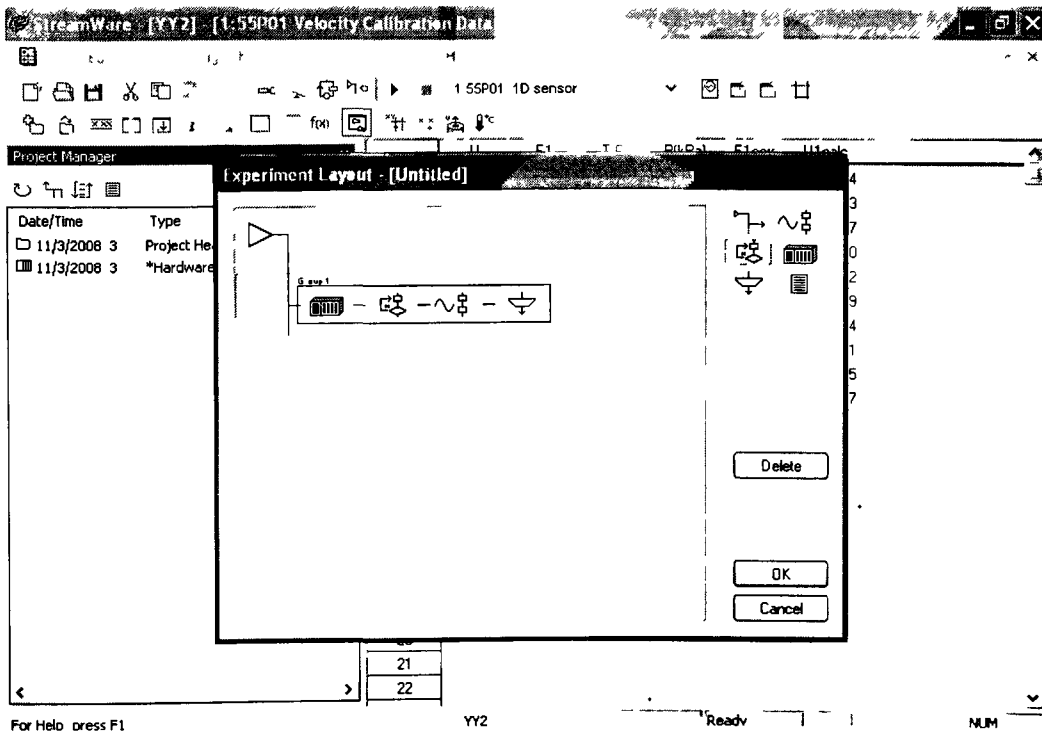
Figure A6 Experiment layout
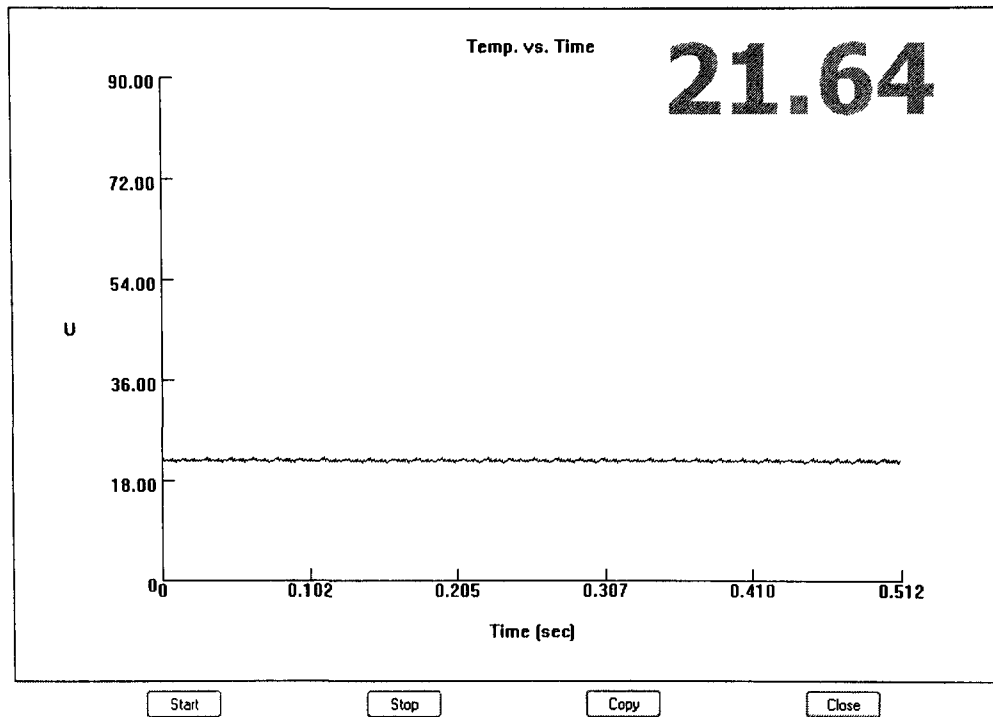
Figure A7 Temperature online analysis

The result of this calibration is
Polynomial fit
[Sensor 1]
C[0]= 135.433823
C[1]= -303.231354
C[2]= 261.014648
C[3]= -106.663643
C[4]= 18.451344

A.2 Matlab Program for 1D-PROBE

```
clc
clear all;

%% #h:#'#:#:#:h:#:#h:h:'h:H#H#4H:'#H#H#:h:#:h:#:h:#h#':H#H#H:#GT/E INPUTS HERE
sample=1600000;

gain=1;
offset=0;
% Calibration Coefficients
c0=-59.097431;
c1=134.270920;
c2=-101.928795;
c3=25.881035;
c4=0.000004;



imax=5;     % Number of Horizontal Traversing Point
jmax=5;     % Number of Vertical Traversing Point

%% ###############################INPUTS ENDS HERE###################


for horizontal=1:imax
    if (horizontal < 10 )
        HH=[int2str(0) int2str(horizontal)];
    else
        HH=[int2str(horizontal)];
    end

    for vertical=1:jmax
        if (vertical < 10 )
            VV=[int2str(0) int2str(vertical)];
        else
            VV=[int2str(vertical)];
        end

        sL=[int2str(1) HH VV];
        disp('Reading file');
        s=[sL ' txt']

        raw=load (s);

        E=raw(1:sample,1);
        E=E/4095*10/gain+offset;
        U=c0+c1*E.^1+c2*E.^2+c3*E.^3+c4*E.^4;

        %%%%%%%%%%%%%%%%%%%%%%%%%%%%%%%%%%%%%

        umean(horizontal,vertical)=mean(U);
        urms(horizontal, vertical)=std(U);
        tu(horizontal,vertical)=100*std(U)/mean(U);
    end
end
```

A.3 Traverse program

Program 1_ vertical motion

```
RUN?
UAI
UBO
hh=11
%% The traversing in the VERTICAL direction will repeat 16 times
vv=10
%% The traversing will move VERTIVALLY FOR TOTAL-1 times at each
HORIZONTAL position
a=1
b=1
O=0
PRINT("VERT1_VERTICAL POSITION")
RP
A=100
V=500000
WHILE a<=hh
C10 WHILE b<=vv
c=UAI
WHILE c==1
UB=1
c=UAI
LOOP
O=0
PRINT("VERT2_VERTICAL POSITION RIGHT BEFORE MOVE")
RP
D=-5000
G
TWAIT
WAIT=10000
UB=0
b=b+1
GOTO10
LOOP
c=UAI
WHILE c==1
UB=1
c=UAI
LOOP
b=b-1
O=0
PRINT("VERT3_VERTICAL POSITION")
RP
```

```
D=5000*b
G
TWAIT
WAIT=20000
UB=0
a=a+1
b=1
LOOP
PRINT("VERT4_PROGRAM VERTICAL ENDS")
END
```

Program 2_ horizontal motion

```
RUN?
UAI
UBO
b=1
hh=10
%% The traversing mechanism will 10 (TOTAL-1) times in the HORIZONTAL
direction.
A=100
V=500000
C10 WHILE b<=hh
c=UAI
WHILE c==1
UB=1
c=UAI
LOOP
PRINT("HORZ1_MOVE HORIZONTALLY ONCE")
D=5000
G
TWAIT
WAIT=20000
UB=0
b=b+1
GOTO10
LOOP
PRINT("HORZ2_HORIZONTAL PROGRAM ENDS")
END
```

Program 3 code for DMA_XFER_1D.exe

```
#include <fstream.h>
#include <stdio.h>
#include <assert.h>
#include <windows.h>
```

```
#include "C:/nidaq/nidaq.h"
#include "C:/nidaq/nidaqcns.h"

short status;
const short port=0, deviceNumber=1, dir_in=0, dir_out=1, line_A_1=0, line_B_1=1,
line_A_2=2, line_B_2=3;
const ready=0, not_ready=1;
short *state_MH = new short, *state_MV = new short;

int Collect_Data_2d(char* binary_indicator, double SampleRate, unsigned long
SampleNumber, short inputMode, char *folderName, int zone, int count_Horizontal, int
count_Vertical);
void Collect_Data_1d(double SampleRate, unsigned long SampleNumber, short
inputMode, char *folderName, int zone, int count_Horizontal, int count_Vertical);
char* get_filename (char* folderName, int zone, int count_Horizontal, int
count_Vertical);
void Save_Data_2d(char* binary_indicator,unsigned long count, short* buffer, char*
filename, short *reading);
void Save_Data_1d(unsigned long count, short* buffer, char* filename,short *reading);
int main()
{
        cout<<"No. of point in the vertical direction: ";
        int vertical_limit;
        cin>>vertical_limit;
        cout<<"No. of point in the horizontal direction: ";
        int horizontal_limit;
        cin>>horizontal_limit;

        //The folreadying sets the communication lines 0, 1, 2, 3.
        cout<<"\nSample Rate (Hz): ";
        double SampleRate;
        cin>>SampleRate;
        cout<<"\nSample Number: ";
        unsigned long SampleNumber;
        cin>>SampleNumber;
        cout<<"\nZone No.: ";
        int zone;
        cin>>zone;
        cout<<"\nFolder Name: ";
        char *folderName = new char[80];
        cin>>folderName;
        cout<<"\nInput MODE (0 diff 1 RSE 2 NRSE): ";
        short inputMode;
        cin>>inputMode;
        cout<<"\nSave data in binary format(Y or N): ";
        char *binary_indicator = new char;
```

```cpp
cin>>binary_indicator;

//This output is WRT the daq board->motor
status = DIG_Line_Config(deviceNumber, port, line_A_1, dir_out);
assert(status==0);

//make sure there is no horizontal traversing
status=DIG_Out_Line(1, 0, 0, 1);
assert(status==0);

//This input is WRT the daq board->motor
status = DIG_Line_Config(1, 0, 1, 0);
assert(status==0);

//This output is WRT the daq board->motor
status = DIG_Line_Config(1, 0, 2, 1);
assert(status==0);


//make sure there is no horizontal traversing
status=DIG_Out_Line(1, 0, 2 1);
assert(status==0);

//This input is WRT the daq board->motor
status = DIG_Line_Config(1, 0, 3, 0);
assert(status==0);

//Preparation is done, real work starts from here
for(int count_Horizontal = 1; count_Horizontal<=horizontal_limit;
count_Horizontal++)
    {
        for (int count_Vertical=1; count_Vertical<=vertical_limit;
count_Vertical++)
            {
                printf("\n%d   %d",count_Horizontal, count_Vertical);


                Collect_Data_1d(SampleRate, SampleNumber, inputMode,
                folderName, zone, count_Horizontal, count_Vertical);

                //activate the traversing, move to next position
                status=DIG_Out_Line(1, 0, 0, 0):
                assert(status==0);

                //get the status of the traversing, move done or not?
                status=DIG_In_Line(1, 0, 1, state_MV);
```

```
                    assert(status==0);

                    //Test whether or not the probe is in position
                    while (*state_MV==1)
                    {
                            status=DIG_In_Line(1, 0, 1 , state_MV);
                            assert(status==0);
                    }//move is done,start new data collection

                    //make sure does not traverse vertically
                    status=DIG_Out_Line(1, 0, 0, 1);
                    assert(status==0);
            }//traversing will return to its vertical origin, since line_A_1 is ready.
            //at this poit, the port A_1 is in ready status, port B_1 is at 0 (READY
            FOR DATA //COLLECTION) status.

            //it's time to make a horizontal traversing

            //activate the traversing, move to next position
            status=DIG_Out_Line(1, 0, 2,0);
            assert(status==0);

            //get the status of the traversing, move done or not?
            status=DIG_In_Line(1, 0, 3, state_MH);
            assert(status==0);

            //Horizontal traversing should be done at this point. The H motor should
            send back a //ready signal

            //Test whether or not the probe is in position
            while (*state_MH==1)
            {
                    status=DIG_In_Line(1, 0, 3, state_MH);
                    assert(status==0);
            }//move is done,start new data collection

            //activate the traversing, move to next position
            status=DIG_Out_Line(1, 0, 2, 1);
            assert(status==0);
        }
        return 1;
}

char* get_filename (char* folderName, int zone, int count_Horizontal, int
count_Vertical)
{
```

```cpp
        char *filename_return = new char[40];
        strcpy(filename_return,folderName);
        char pZONEc[1];
        char pZEROHc[1];
        char pZEROVc[1];

        char pCOUNT_HORIZONTALc[2];
        char pCOUNT_VERTICALc[2];

        if (count_Horizontal < 10)
        {
                _itoa(0, pCOUNT_HORIZONTALc,10);
                _itoa(count_Horizontal, pZEROHc,10);
                strcat(pCOUNT_HORIZONTALc,pZEROHc);
        }
        else
                _itoa(count_Horizontal,pCOUNT_HORIZONTALc,10);

        if (count_Vertical < 10)
        {
                _itoa(0, pCOUNT_VERTICALc,10);
                _itoa(count_Vertical, pZEROVc,10);
                strcat(pCOUNT_VERTICALc,pZEROVc);
        }
        else
                _itoa(count_Vertical,pCOUNT_VERTICALc,10);

        _itoa(zone,pZONEc,10);
        char *pDotTxt = ".txt";

        strcat(filename_return,pZONEc);
        strcat(filename_return,pCOUNT_HORIZONTALc);
        strcat(filename_return,pCOUNT_VERTICALc);
        strcat(filename_return,pDotTxt);

        pDotTxt = NULL;

        return filename_return;
}


void Collect_Data_1d(double sampleRate, unsigned long SampleNumber, short
inputMode, char *folderName, int zone, int count_Horizontal, int count_Vertical)
{
        short status, deviceNumber=1, chan0=0, chan1=1, gain = 1. inputRange = 10,
polarity=1, driveAIS = 1;
        unsigned long count = SampleNumber;
```

```
        short *buffer = new short[count];
        char *filename = new char[40];
        short *reading = new short[1];
        filename = get_filename (folderName, zone, count_Horizontal, count_Vertical);

        printf("\nPlease wait, data is being collected");
        status = AI_Configure (deviceNumber, chan0, inputMode, inputRange, polarity,
driveAIS);
        assert(status==0);
        status = AI_Configure (deviceNumber, chan1, inputMode, inputRange, polarity,
driveAIS);
        assert(status==0);

        status = DAQ_Op (deviceNumber, chan0, gain, buffer, count, sampleRate);
        printf("%d",status);
        assert(status==0);
        status = AI_Read (deviceNumber, chan1, gain, reading);
        assert(status==0);
        Save_Data_1d(count, buffer, filename, reading);

        printf("\nGo");
}
void Save_Data_1d(unsigned long count, short* buffer, char* filename,short *reading)
{
        printf("\nSaving data to disk.");

        ofstream fout(filename, ios::app);

        for(unsigned long count_data = 0; count_data<count;count_data++)
        {
                fout<<"\n"<<*(buffer+count_data);
        }
        fout<<"\n"<<*reading;
        fout.close();
        printf("\nSavind data completed");
```

Appendix B: load cell Calibration
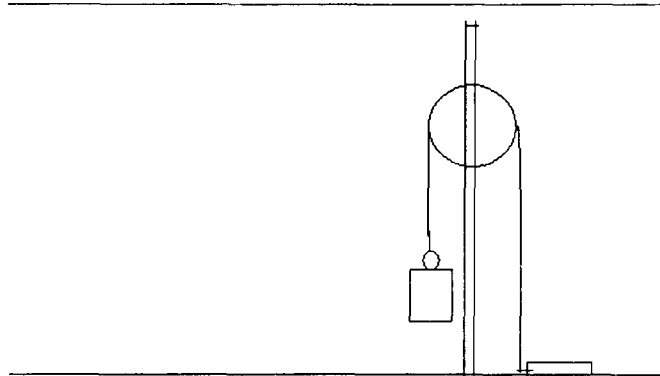
Figure B1 load cell calibration

The upper and lower limits of the load cell need to be adjusted every time before the drag measurement to optimize the sensitivity. During the calibration, load cell was secured on the wind tunnel floor, as shown in Figure B1, a sample pulley system was designed for the calibration, one side of the string was connected to the load cell and the other side was connect to a load, which is 100 gram for the upper limit in our cases. The procedures are,

1 *Press the $>_{(MENU)}$ key to display LO IN (low signal input value).

   Apply an input for a know low value, which is 0 N in our cases,

   *Press $>_{(PEAK)}$ to display the input signal.

   The meter will momentarily blank and then display the low input.

   *Press RESET to store the reading as the low input.

   The result of LO IN in this case is 0.0007mv

2*Press the $>_{(MENU)}$ key to display HI IN (high signal input value).

   Apply an input for a know low value, which is 0.49 N in our cases,

   *Press $>_{(PEAK)}$ to display the input signal.

   The meter will momentarily blank and then display the high input.

   *Press RESET to store the reading as the high input.

The result of HI IN in this case is 0.3085mv.

3 Calculate the equation F (N) = $0.615F_{load\ cell}$ (mV).

Which shows the relationship between the net force applied on the string and the load cell data which was delivered in mili-voltage from the amplifier

Appendix C: Sampling Frequency/Number selecting

The sampling frequency is determined by the maximum frequency component in the flow. In order to meet Nyquist–Shannon sampling theorem, the sampling frequency has been chosen as $2 \times f_{cutting}$ or $2.5 \times f_{cutting}$, this cutting frequency can be obtained in the "square wave test" during calibration. The square wave test is conducted under the potential maximum velocity of the measurement. For our case, the maximum velocity is around 15m/s, and the corresponding cutting frequency is around 30 kHz, theoretically, the sampling frequency should be 60 or 75 kHz.
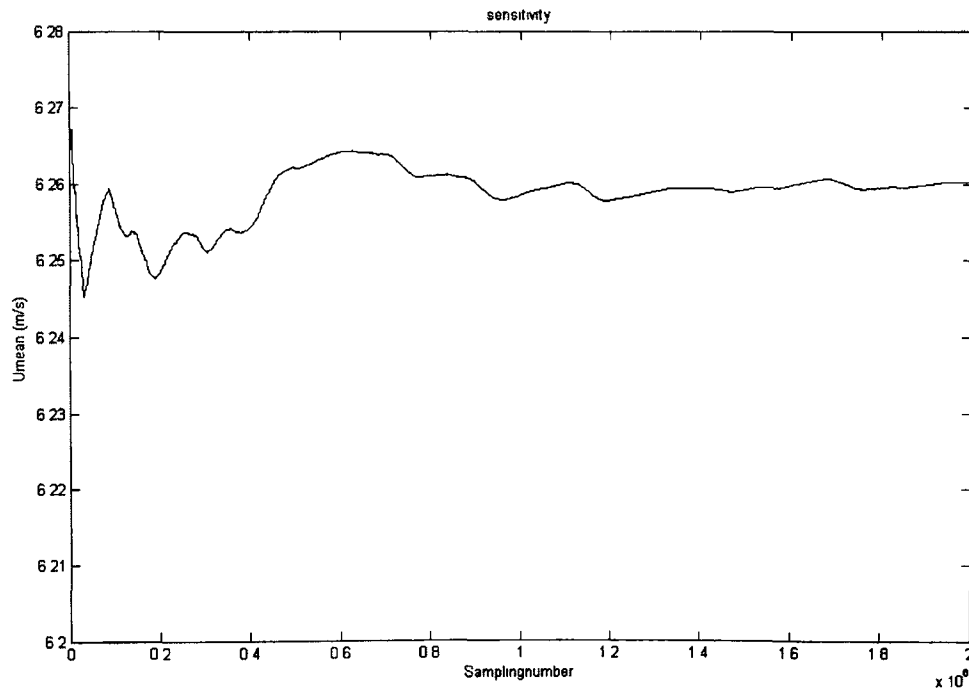
Figure C1 mean velocity vs. sampling number (x=1:1: sampling number)

From Figure C1, it seems after 1.6×10^6, the time averaged velocity tends to be uniform

Appendix D: Uncertainty Analyses

Uncertainty of Velocity

The uncertainty of each velocity sample is determined by non-statistical means based on detailed knowledge about the instrumentation, calibration equipment and experimental conditions. In our cases, two velocity sample were chosen to calculate the uncertainly, which are V_1=6.0215m/s and V_2=13.9824m/s.

The source of Uncertain is mainly consisted of three part, Calibration equipment, Linearization (Conversion) and A/D board resolution. The other factors such as ambient pressure, humidity are neglected because of the relative small standard uncertainty.

a) Calibration equipment

The calibrator uncertainty is often given as a *relative standard* uncertainty, a_{cal}, in percent plus a constant contribution b_{cal} in m/s :

$$STDV(U_{calibrator}) =\pm a (\%)+b(m/s)$$

Table D1 Comparison of auto calibration and calibration with Pitot   static tube

	a (%)	b (m/s) when U<5m/s
auto calibrator	±1	±0.02
calibration with pitot-static tube	±2	N/A

In our cases, both velocities are larger than 5m/s, and the results are obtained from the auto calibrator, so 1% should be used in the following calculation.

b) Linearisation (Conversion)

$STDV(\nabla U_{lin})$ is the standard deviation of the curve fitting errors in the calibration points in %. Which are 0.298% and 0.376% for V_1 and V_2 respectively.

c) A/D board resolution

Calculation of $\dfrac{1}{U}\dfrac{E_{AD}}{2^n}\dfrac{\partial U}{\partial E}$ under the velocity samples of V_1=6.0215m/s and V_2=13.9824m/s

U=6.0215m/s, E_{AD}=10volts, n=12bit,

$U = c0 + c1 \times E + c2 \times E^2 + c3 \times E^3 + c4 \times E^4$,

Where,

c0= -55.320591;

c1= 128.169662;

c2= -99.292603;

c3= 25.725582;

c4= 0.000001;

So,

For V_1=6.0215m/s

$$\frac{1}{U} \frac{E_{AD}}{2^n} \frac{\partial U}{\partial E} = 0.015$$

V_2=13.9824m/s

$$\frac{1}{U} \frac{E_{AD}}{2^n} \frac{\partial U}{\partial E} = 0.011$$

The relative expanded uncertainties on a single velocity sample obtained with a single-sensor hot-wire probe in air, can be summarized in the following table:

Table D2 Uncertainties on a single velocity sample

Source of uncertainty	Input variants		Typical value ΔX_i	Relative output varians	Typical value $\Delta Y_i/U$	Coverage factor k	Relative standard uncertain-ty $\Delta Y_i/kU$
Calibration	U_1	ΔU_{cal}	1%	$2STDV(100\Delta U_{cal})$	0.02	2	0.01
	U_2		1%		0.02		0.01
Linearization	U_1	ΔU_{fit}	0.298%	$2STDV(100\Delta U_{fit})$	0.00596	2	0.00298
	U_2		0.376%		0.00752		0.00376
A/D resolution	E_{AD}		10 volts	$\frac{1}{U}\frac{E_{AD}}{2^n}\frac{\partial U}{\partial E}$	0.015	$\sqrt{3}$	0.008
	n		12 bit		0.011		0.006
Relative expanded uncertainty	U1=0.027=2.7% U2=0.024=2.4%						

Thus,

$V_1 = 6.0215 \pm 0.16$ m/s
$V_2 = 13.9824 \pm 0.33$ m/s

The calculation is followed the procedure provided in [How to measure turbulence with hot-wire anemometers- a practical guide], Finn E. Jorgensen ,dantec dynamic literature, 2002

Uncertainty of Drag Force

The drag force in this project was measured by using a load cell. The uncertainty in the drag measurement was deduced from four different sources, i.e. the front area of truck model measurement, the velocity measurement, the air density calculation, and the load cell measurement. The dimension of the truck model was measured by using a micrometer, which has a resolution of 0 001 mm. Meanwhile, repeating measurements lead to a repeatability uncertainty of ±0.2 mm. Thus, the total uncertainty of the front area of the truck model was 1.6%. The uncertainty in the mean velocity measurement by Pitot - static tube is 3.1%. The load cell has a resolution of 0.0001 (mV) and uncertainty of 7.4%. The uncertainty in the calculation of the air density was negligible comparing to other factors. To sum up, the drag coefficient C_D was calculated from $C_D = F_D / \left[1/2\rho U^2 A \right]$, the nominal uncertainties of drag coefficient was almost 8.7% in this study.

Appendix E Boundary Layer Effect

The ground boundary layer can distort the velocity profile in wake area behind the trailer, as well as the drag force applied on the truck model which is secured on the wind tunnel floor. To reduce the boundary layer effect, an elevated plate with a dimension of L_{plate} (60in) $\times W_{plate}$ (29in) $\times$ T (0.75in) was located 30 inch downstream the inlet of the wind tunnel test section. The ground clearance of elevated plate was set to be 6 inch after several trials.

Without elevated plate

The location was chosen at the centre line 85 inch downstream the inlet of the wind tunnel test section. 21 points were measured from 0.5 inch to 5.5 inch above the wind tunnel floor. Results are shows in Figure E1.
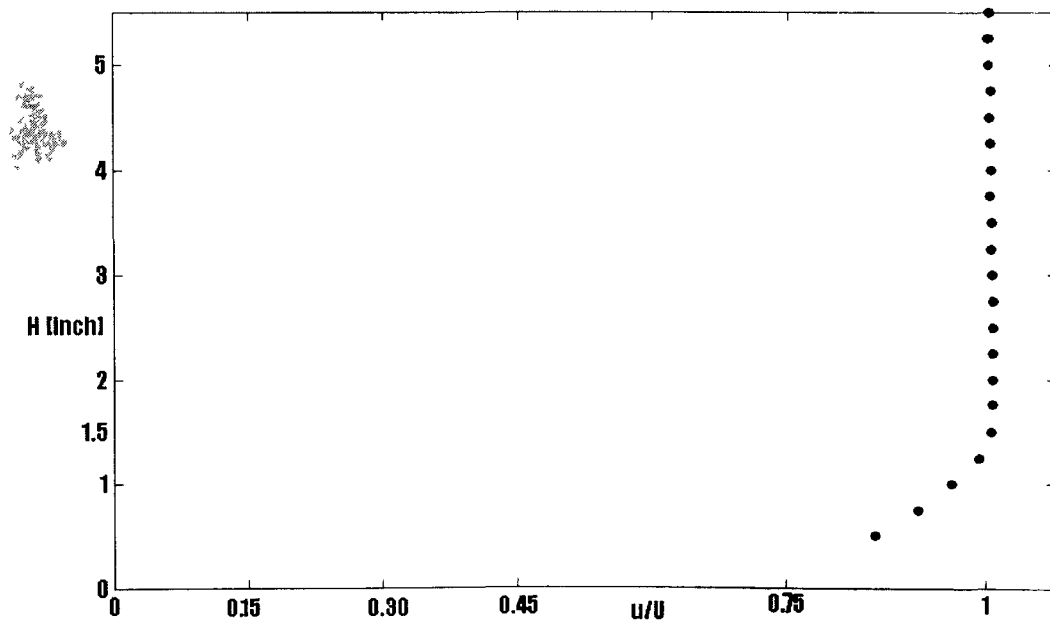
Figure E1 Velocity profiles 85 inch downstream the inlet of the wind tunnel
Boundary layer thickness (δ=1.5 inch)

With elevated plate

The location was chosen at the centre line 55 inch downstream from the leading edge of the elevated plate. 13 points were measured from 0.5 inch to 2.7 inch above the plate. Results are shown in Figure E2.
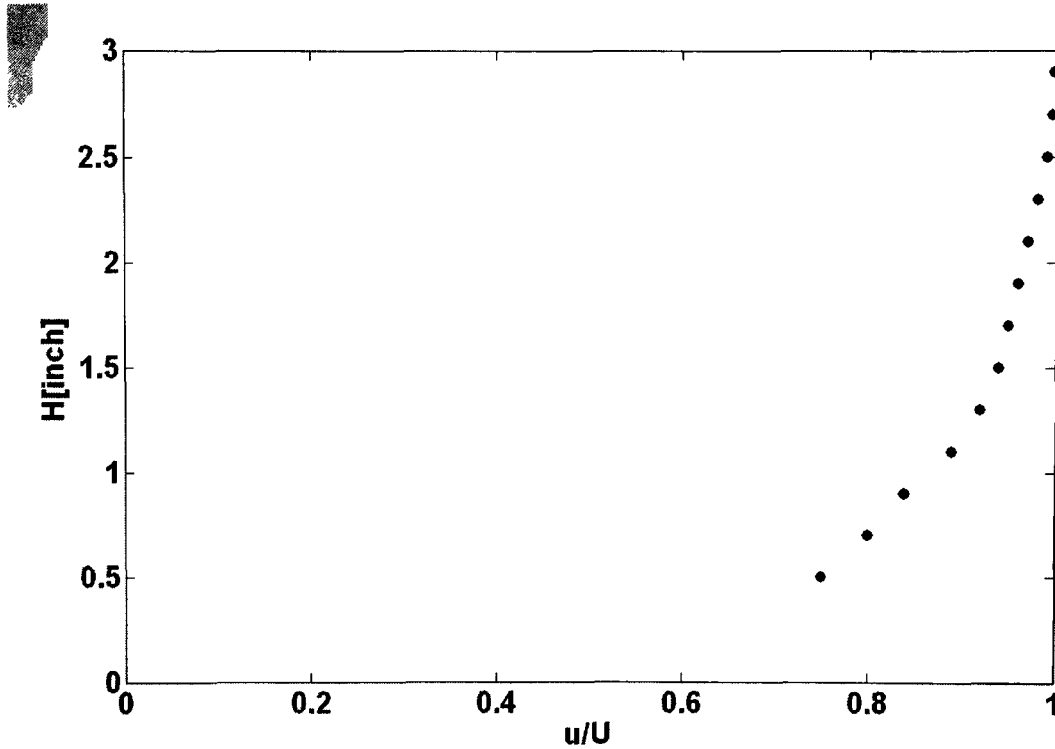
Figure E2 Velocity profiles 55 inch downstream of the elevated plate leading edge

From Figure E2, it can be seen that boundary layer can not be eliminated but slightly changed by applying the elevated plate.

Appendix F Blockage Ratio Effect

In wind tunnel study, the blockage ratio $\varphi = A/A_N$, where A is the frontal area of the vehicle shown in Figure F1 below, and A_N is the cross-sectional area of wind tunnel test section. In order to provide kinematic similarity of the flow in a tunnel to that on road, the blockage ratio φ, which is zero on the road, should be as small as possible. However, cost considerations of a tunnel (construction and operation) could only offer a blockage ratio as large as "feasible."
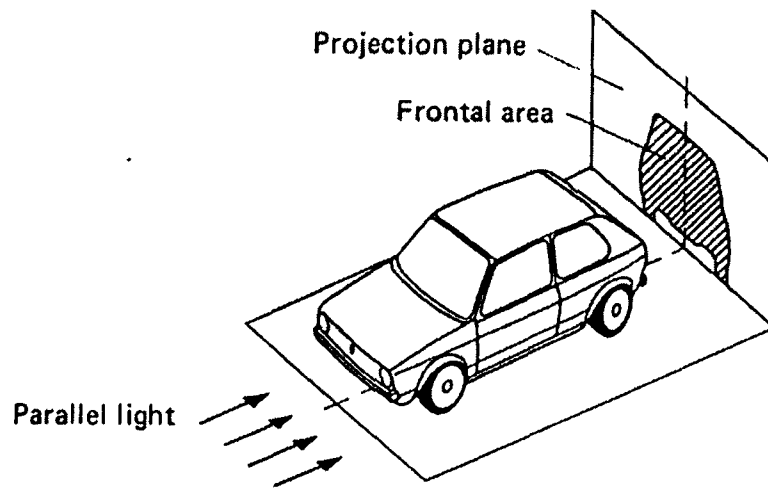
Figure F1: Definition of frontal area of a vehicle

In this project, the truck model has a frontal area of $A=0.0187m^2$ (0.108m× 0.173m) and the cross-sectional area of the wind tunnel is $A_N=0.5776$ m^2, thus the blockage ratio is $\varphi=3.2\%$. To reduce the boundary layer effect, an elevated plate was applied in the test section. With the elevated plate, $A_N=0.5631$ m^2, φ goes up to 3.3%,(The method of blockage ratio calculation is developed by [Garry, 1991]), which is still less than the upper limit of 5% blockage ratio, beyond which corrections of blockage effect should be applied [Hucho 1998].
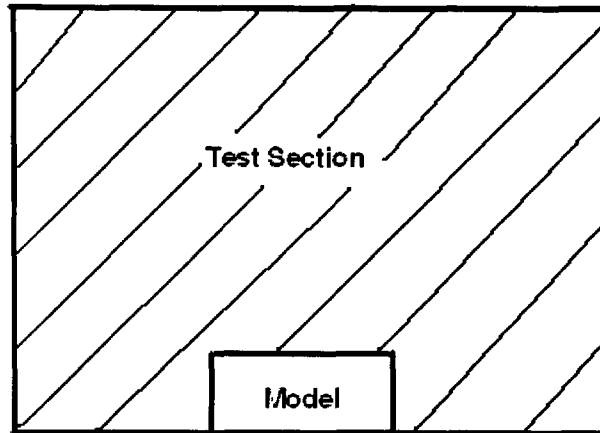
Figure F2: Test section without elevated plate

$A_N = 0.76m \times 0.76m = 0.5776 \ m^2$

$\varphi = A/A_N = 0.0187/0.5776 = 3.2\%$
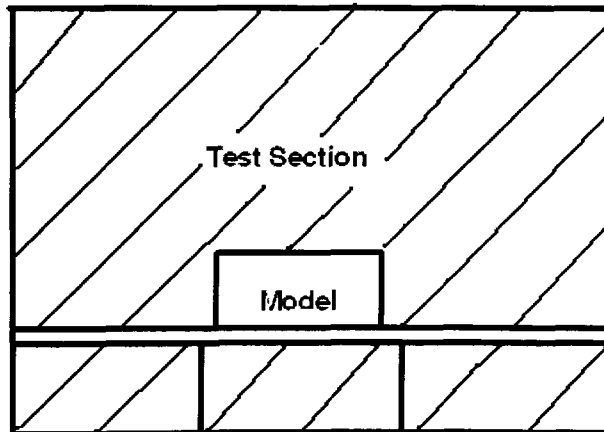
Figure F3: Test section with elevated plate

Thickness of the plate=0.019m

$A_N = (0.76-0.019) \ m \times 0.76m = 0.5631 \ m^2$

$\varphi = A/A_N = 0.0187/0.5631 = 3.3\%$

The blockage ratio at $\pm \ 5°$ yaw angle

$A = 0.0187 \ m^2 \times \tan5° + 0. \ 0187 \ m^2 = 0. \ 0203 \ m^2$

$\varphi = A/A_N = 0.0203/0.5631 = 3.6\%$

VITA AUCTORIS

1982   Born in Changchun, Jilin, P.R China.

2001   Completed high school at Middle School Attached to Northeast University, Changchun, P.R China.

2006   Received Bachelor Degree of Automotive Engineering at Jilin University, Changchun, P.R China.

2009   Currently a candidate for the degree of Master of Applied Science in Mechanical Engineering at the University of Windsor, Windsor, Ontario, Canada.